

# OD-DEAL: Dynamic Expert-Guided Adversarial Learning with Online Decomposition for Scalable Capacitated Vehicle Routing

Dongbin Jiao<sup>1</sup> Zisheng Chen<sup>1</sup> Xianyi Wang<sup>1</sup> Jintao Shi<sup>1</sup> Shengcai Liu<sup>2</sup> Shi Yan<sup>1</sup>

## Abstract

Solving large-scale capacitated vehicle routing problems (CVRP) is hindered by the high complexity of heuristics and the limited generalization of neural solvers on massive graphs. We propose OD-DEAL, an adversarial learning framework that tightly integrates hybrid genetic search (HGS) and online barycenter clustering (BCC) decomposition, and leverages high-fidelity knowledge distillation to transfer expert heuristic behavior. OD-DEAL trains a graph attention network (GAT)-based generative policy through a minimax game, in which divide-and-conquer strategies from a hybrid expert are distilled into dense surrogate rewards. This enables high-quality, clustering-free inference on large-scale instances. Empirical results demonstrate that OD-DEAL achieves state-of-the-art (SOTA) real-time CVRP performance, solving 10000-node instances with near-constant neural scaling. This uniquely enables the sub-second, heuristic-quality inference required for dynamic large-scale deployment.

## 1. Introduction

The capacitated vehicle routing problem (CVRP) is a fundamental NP-hard challenge in modern logistics and supply chain management (Toth & Vigo, 2014; Laporte, 2024; Xu et al., 2025). Due to the combinatorial explosion of the search space, traditional exact and heuristic solvers encounter prohibitive computational overhead on large-scale instances (Liu et al., 2021; Bogrybayeva et al., 2024).

Neural combinatorial optimization (NCO) has recently emerged as a transformative paradigm, leveraging deep

learning to approximate optimal routing policies with end-to-end neural inference (Wu et al., 2024). Despite their speed, current neural solvers face a critical scalability-optimality bottleneck: supervised approaches are often restricted by static, expensive labels, while reinforcement learning (RL) methods typically suffer from sparse reward signals and poor generalization (Bello et al., 2017; Gunarathna et al., 2022; Liu et al., 2023). Furthermore, standard Transformer-based architectures frequently are prone to mode collapse, limiting solution diversity and structural integrity on massive graphs.

To address these limitations, generative flow networks (GFlowNets) (Bengio et al., 2021a; Zhang et al., 2023) have been proposed to sample diverse trajectories with probabilities proportional to a reward function. Recent flow-based models, such as AGFN (Zhang et al., 2025) improves solution diversity, but it lacks the structural inductive biases and expert regularization required for large-scale optimization. By neglecting local signals in favor of holistic objectives, such solvers fail to capture fine-grained structures, resulting in suboptimal performance ceilings and reduced training stability.

In this work, we propose OD-DEAL, an expert-guided adversarial learning framework with online decomposition. Grounded in the GFlowNet paradigm, OD-DEAL bridges the gap between the inference efficiency of neural methods and the solution quality of state-of-the-art (SOTA) heuristics. Unlike standard RL, OD-DEAL reformulates route construction as a stochastic flow matching problem. By utilizing the trajectory balance (TB) objective, the model learns a policy that ensures precise distributional alignment with a high-performance expert manifold.

At the core of our framework is a graph attention network (GAT) generator, specifically designed to capture the intricate, non-linear dependencies between long-range spatial proximity, heterogeneous customer demands, and residual vehicle capacity. To overcome reward sparsity, we introduce a dynamic expert oracle that synergizes hybrid genetic search (HGS) (Vidal et al., 2012) with online barycenter clustering (BCC) decomposition (Santini et al., 2023). This oracle provides high-fidelity demonstrations of “divide-and-conquer” logic, which are distilled into the generator via an

<sup>1</sup>School of Information Science and Engineering, Lanzhou University, Lanzhou 730000, P. R. China (Emails: {jiaodb, chzisheng2024, wxianyi2025, shjt2024}@lzu.edu.cn)

<sup>2</sup>Guangdong Provincial Key Laboratory of Brain-Inspired Intelligent Computation, Department of CSE, SUSTech, Shenzhen 518055, P. R. China. Correspondence to: Shengcai Liu <yanshi@lzu.edu.cn>, Shi Yan <liusc3@sustech.edu.cn>.

adversarial minimax framework. Through a minimax game against a learned discriminator, the generator distills this decomposition logic into dense surrogate rewards, allowing the policy to internalize strategic partitioning and local search without explicit clustering at runtime. Empirical results demonstrate that OD-DEAL achieves SOTA real-time CVRP performance through near-constant neural scaling to large-scale instances.

Our contributions are as follows: (i) We propose OD-DEAL, which integrates a GAT within an adversarial GFlowNet framework to model complex spatial-demand dependencies for end-to-end VRP inference. (ii) We introduce a hybrid expert oracle synergizing HGS with online BCC decomposition. This “divide-and-conquer” strategy enables the generator to implicitly internalize complex topological logic. (iii) Experimental results show that OD-DEAL achieves a real-time CVRP SOTA through GAT-based modeling and expert distillation of decomposition-augmented heuristics. It scales near-constantly to 10000 nodes, providing the sub-second, heuristic-quality inference essential for dynamic large-scale deployment.

## 2. Related Work

**Heuristics and Decomposition for Large-scale VRP.** The SOTA in VRP is currently defined by heuristics such as HGS (Vidal et al., 2012; Vidal, 2022) and LKH-3 (Helsgaun, 2017). These solvers achieve near-optimal accuracy through sophisticated local search and population-based diversity management. However, they encounter a “scalability wall” as the combinatorial search space expands, rendering global optimization on massive instances computationally prohibitive. To mitigate this, research has shifted toward decomposition strategies (Zong et al., 2022; Santini et al., 2023; Ye et al., 2024; Zheng et al., 2024b; Kerscher & Minner, 2025; Zheng et al., 2025), specifically clustering-based approaches that partition global problems into tractable subproblems. OD-DEAL leverages these high-performance heuristics not as standalone solvers, but as a dynamic expert oracle to provide high-fidelity supervisory signals for neural training.

**Neural Combinatorial Optimization (NCO).** NCO reframes the VRP as a data-driven policy approximation problem (Bengio et al., 2021b; Zheng et al., 2024a). Constructive neural solvers typically utilize graph neural networks (GNNs) or Transformers to generate solutions end-to-end (Kool et al., 2019; Kotary et al., 2021; Cappart et al., 2023; Luo et al., 2025). While architectures like GAT effectively capture heterogeneous node features and spatial dependencies (Bui & Mai, 2023; Cappart et al., 2023; Luo et al., 2023), most solvers rely on policy gradient methods (e.g., REINFORCE (Williams, 1992)) that struggle with sparse reward signals and poor generalization to large-scale distri-

butions (Bengio et al., 2021b; Wu et al., 2024; Yao et al., 2025). Furthermore, standard architectures often suffer from mode collapse, failing to represent the multimodal nature of optimal routing for large-scale CVRP. We address these limitations by adopting the GFlowNet paradigm (Bengio et al., 2023), which facilitates robust exploration and better represents the solution distribution through flow consistency.

## ADVERSARIAL LEARNING AND KNOWLEDGE DISTILLATION

Knowledge distillation (KD) via imitation learning is a common approach to bridge the gap between heuristic precision and neural speed (Bi et al., 2022; Sun & Yang, 2023; Bogolyubayeva et al., 2024). However, pure imitation often suffers from exposure bias and fails to generalize when the student deviates from expert trajectories. GflowNets mitigates this by framing optimization as a distribution matching task rather than point-wise replication, compelling the model to internalize the underlying structural manifold of expert-like solutions (Kim et al., 2024; 2025). Recent advancements, such as AGFN (Zhang et al., 2025; Zhang & Cao, 2025), integrate adversarial objectives with flow-based sampling to provide denser training signals. OD-DEAL differentiates itself by integrating a decomposition-augmented expert directly into the adversarial loop. By coupling the structural discriminative power of generative adversarial networks (GANs) with the scalability of clustering-based heuristics, our framework internalizes high-level “divide-and-conquer” logic, ensuring both inference efficiency and near-optimal performance at large-scale.

## 3. Preliminaries

**CVRP Definition.** The CVRP is generally defined over a complete graph  $G(V, E)$ , where  $V = \{v_0\} \cup V_c$  consists of a single depot  $v_0$  and  $N$  customer nodes  $V_c = \{v_1, \dots, v_N\}$ . Each edge  $(i, j) \in E$  is associated with a non-negative travel cost  $c_{ij}$ , and each customer  $i \in V_c$  has a non-negative demand  $d_i$ . A fleet of  $K$  identical vehicles, each with capacity  $Q$ , is available to service the customers. The CVRP seeks to identify a set of optimal vehicle trajectories that minimize the aggregate cost  $\sum c_{ij}$  subject to: (i) each customer is assigned to exactly one route, (ii) the sum of demands on every route does not exceed the vehicle capacity  $Q$ , and (iii) all routes starting and ending at the depot. A comprehensive integer linear programming (ILP) formulation, is provided in Appendix Sections A.1 and E.1.

**Learning to Solve CVRPs.** NCO models the CVRP as an autoregressive process where a policy  $P_\theta(a|s) = \prod_{t=1}^T p_\theta(a_t|s, a_{<t})$  is typically optimized to maximize expected rewards. However, traditional RL faces reward sparsity and search space explosion at scale. To address these bottlenecks, we propose OD-DEAL, an adversarial frame-

work that distills expert decomposition strategies into the generative policy. By aligning  $\pi_\theta$  with an expert distribution  $P_E$  derived from HGS-BCC decomposition, the model internalizes latent “divide-and-conquer” logic. This allows OD-DEAL to perform high-quality, clustering-free inference on massive graph topologies, significantly improving generalization robustness and accuracy while maintaining sub-second efficiency. Details of the OD-DEAL framework are given in Appendix C.1.

## 4. Methodology

### 4.1. Generator: GAT-Based Policy Network

The generator  $\pi_\theta$  serves as the key decision-making component of OD-DEAL, designed to perform autonomous inference upon completion of training. To overcome the representational limitations of traditional GNNs in capturing complex node interactions, we adopt a GAT backbone (Veličković et al., 2018). The GAT utilizes a multi-head self-attention mechanism to adaptively assign importance to neighboring nodes based on their latent features. This dynamic weighting is uniquely suited for the CVRP, as it enables the model to capture the complex interdependencies among spatial proximity, heterogeneous customer demands, and residual vehicle capacity. By effectively aggregating these heterogeneous node features, the GAT produces highly expressive representations that are essential for constructing high-quality routing solutions. Detailed specifications of the GAT architecture are provided in Appendix B.

#### 4.1.1. STRUCTURAL ENCODER

A multi-layer GAT is adopted to encode both topological and attribute-based features of the CVRP instance, capturing intricate dependencies between nodes to generate high-dimensional node embedding vectors  $\mathbf{h}_i \in \mathbb{R}^{D_{\text{units}}}$ . The encoding workflow is executed in the following three stages.

**Initial Feature Transformation.** To harmonize input features of varying dimensions, we first apply independent linear projections to the raw node features  $\mathbf{x}_i$  and edge features  $\mathbf{a}_{ij}$ . This maps them into a unified hidden dimension  $D_{\text{units}}$ , providing a standardized input for the attention mechanism:

$$\mathbf{h}_i^{(0)} = \sigma(\mathbf{W}_{\text{node}} \mathbf{x}_i + \mathbf{b}_{\text{node}}), \quad (1)$$

$$\mathbf{e}_{ij} = \sigma(\mathbf{W}_{\text{edge}} \mathbf{a}_{ij} + \mathbf{b}_{\text{edge}}), \quad (2)$$

where  $\mathbf{W}_{\text{node}}$  and  $\mathbf{W}_{\text{edge}}$  are trainable weight matrices,  $\mathbf{b}_{\text{node}}$  and  $\mathbf{b}_{\text{edge}}$  are bias vectors, and  $\sigma(\cdot)$  denotes a non-linear activation function.

**Node Representation Update.** The encoder consists of  $L$  stacked GAT layers. In each layer, the model performs message passing by computing attention scores based on the source node, its neighbors, and the associated edge features.

For each attention head, the unnormalized correlation score  $s_{ij}^{(k,h)}$  between node  $i$  and  $j$  is computed as:

$$s_{ij}^{(k,h)} = \text{AttentionMech}^{(k,h)}(\mathbf{h}_i^{(k)}, \mathbf{h}_j^{(k)}, \mathbf{e}_{ij}). \quad (3)$$

To ensure a probabilistic interpretation and facilitate comparison across the neighborhood  $\mathcal{N}(i)$ , these scores are normalized using the softmax function to obtain the attention coefficients  $\alpha_{ij}^{(k,h)}$ :

$$\alpha_{ij}^{(k,h)} = \text{softmax}_j(s_{ij}^{(k,h)}). \quad (4)$$

These coefficients  $\alpha_{ij}^{(k,h)}$  signify the relative importance of neighbor  $j$  to node  $i$  within the  $h$ -th subspace.

**Multi-head Aggregation.** Finally, the encoder aggregates the neighborhood information via multi-head attention. To stabilize the learning process and mitigate the risk of vanishing gradients in deep architectures, we incorporate residual connections and batch normalization:

$$\mathbf{h}_i^{(k+1)} = \mathbf{h}_i^{(k)} + \text{BN}^{(k)}\left(\sigma\left(\mathbf{h}_{\text{aggr},i}^{(k+1)}\right)\right), \quad (5)$$

where  $\mathbf{h}_{\text{aggr},i}^{(k+1)}$  represents the concatenated or averaged output from the multiple attention heads. After  $L$  iterations, the final embedding  $\mathbf{h}_i$  encapsulates the global topological structure of the graph, providing a context-rich representation for the subsequent sequential decision-making process.

### 4.2. Sequential Constructive Decoder

The decoder in OD-DEAL follows an auto-regressive paradigm, parameterizing a policy network  $\pi_\theta(a_t|s_t)$  to incrementally construct feasible solution sequences.

At each decoding step  $t$ , let  $v_i$  denote the currently visited node. The decoder evaluates the propensity of transitioning to a candidate neighbor  $v_j$  by leveraging the rich node embeddings learned by the GAT encoder. Specifically, we construct a relational context vector  $f_{ij}$  by concatenating the source and target embeddings, which is then mapped to a scalar logit  $u_{ij}$  via a multi-layer perceptron (MLP):

$$f_{ij} = [\mathbf{h}_i \parallel \mathbf{h}_j], \quad u_{ij} = \text{MLP}_{\theta_{\text{dec}}}(f_{ij}), \quad (6)$$

where  $[\cdot \parallel \cdot]$  represents the concatenation operation. This context vector  $f_{ij}$  captures the heterogeneous dependencies between spatial proximity and demand-capacity interactions. To strictly enforce the hard constraints of the CVRP (i.e., single visitation and capacity limits), we incorporate a dynamic masking mechanism. A mask  $M_{ij}^{(t)}$  is applied to the raw logits, defined as:

$$M_{ij}^{(t)} = \begin{cases} 0 & \text{if } v_j \in \mathcal{N}_{\text{valid}}(s_t) \\ -\infty & \text{otherwise} \end{cases}, \quad (7)$$

**Algorithm 1** Expert Solutions via BCC Decomposition

---

```

1: Input: Initial Solution  $R_{\text{init}}$ , Node Coordinates  $X$ , Demands  $D$ , Vehicle Capacity  $Q$ , Target Subproblem Size  $m$ .
2: Output: Refined Global Solution  $R_{\text{final}}$ , Total Cost  $C_{\text{final}}$ .
3: // Phase 1: Route-Based Spatial Decomposition
4:  $N \leftarrow \text{CountCustomers}(R_{\text{init}})$ 
5: // Determine number of subproblems
6:  $k \leftarrow \lceil N/m \rceil$ 
7:  $B \leftarrow \text{ComputeBarycenters}(R_{\text{init}}, X)$ 
8:  $\text{Labels} \leftarrow \text{KMeans}(B, k)$ 
9: // Partition into independent clusters  $\{C_1, \dots, C_k\}$ 
10:  $C \leftarrow \text{GroupRoutesByLabel}(R_{\text{init}}, \text{Labels})$ 
11: // Phase 2: Parallel Subproblem Solving
12:  $\text{Solutions} \leftarrow \text{List of size } k$ 
13: for all cluster  $C_i$  in  $C$  with index  $i$  do {in parallel}
14:   // Map global  $v_{\text{id}}$  to local  $[0, n']$ 
15:    $V_{\text{sub}}, \mathcal{M} \leftarrow \text{BuildMapping}(C_i, v_0)$ 
16:   // Constraint: Vehicle count matches route count
17:    $K_{\text{sub}} \leftarrow |C_i|$ 
18:    $\text{Data}_{\text{sp}} \leftarrow \text{CreateInstance}(V_{\text{sub}}, D, X, Q, K_{\text{sub}})$ 
19:   // Solve subproblem
20:    $R_{\text{local}} \leftarrow \text{SolveHGS}(\text{Data}_{\text{sp}})$ 
21:   // Store optimized routes with global IDs
22:    $\text{Solutions}[i] \leftarrow \text{MapToGlobal}(R_{\text{local}}, \mathcal{M})$ 
23: end for
24: // Phase 3: Global Merge
25:  $R_{\text{final}} \leftarrow \emptyset$ 
26: for all  $R_{\text{part}}$  in  $\text{Solutions}$  do
27:    $R_{\text{final}} \leftarrow R_{\text{final}} \cup R_{\text{part}}$ 
28: end for
29:  $C_{\text{final}} \leftarrow \text{CalculateCost}(R_{\text{final}})$ 
30: return  $R_{\text{final}}, C_{\text{final}}$ 

```

---

where  $\mathcal{N}_{\text{valid}}(s_t)$  represents the set of unvisited nodes that satisfy the residual vehicle capacity constraint. The selection probability is then derived via a softmax distribution over the masked logits:

$$p(a_t = v_j | s_t) = \frac{\exp(u_{ij} + M_{ij}^{(t)})}{\sum_{k \in \mathcal{P}} \exp(u_{ik} + M_{ik}^{(t)})}. \quad (8)$$

To balance between exploration and exploitation under the GFlowNet objective, we adopt a hybrid decoding mechanism (Zhang et al., 2025). During training, we employ an  $\epsilon$ -greedy strategy with  $\epsilon = 0.05$ , where the model selects the greedy action with probability 0.95 and samples stochastically from  $p(\cdot | s_t)$  with probability 0.05 to ensure diverse state-space exploration. At inference time, we perform parallel rollouts (e.g., 100 trajectories) and select the solution with the minimum cost, balancing exploration of the search space with high-quality solution construction.

### 4.3. Expert Policy: Decomposition-Augmented HGS

The expert policy  $P_E$  serves as a high-fidelity supervisory oracle distills high-quality local and global routing logic into a performance upper bound, providing the target distribution for training the generator.

**Heuristic Selection.** We utilize the HGS (Vidal et al., 2012) as the foundational expert algorithm. HGS is widely recognized as a SOTA metaheuristic for the CVRP, achieving superior performance by synergizing the global exploration capabilities of genetic algorithms with the intensive exploitation of sophisticated local search procedures.

**Large-Scale Decomposition Strategy.** Despite its effectiveness on standard benchmarks, standalone HGS experiences performance degradation when applied directly to large-scale instances due to the exponential expansion of the search space (Santini et al., 2023). To maintain solution quality at scale, we incorporate a “divide-and-conquer” framework based on BCC. As a route-based decomposition strategy, BCC offers high robustness by partitioning the problem into manageable sub-topologies while preserving the integrity of individual routes (Santini et al., 2023).

**Expert Solution Generation.** The generation of the expert solution  $S_{\text{expert}}$  follows a three-stage process, as detailed in Algorithm 1: (i) *Decomposition phase*: Given an initial feasible solution  $R_{\text{init}}$ , we calculate the barycenter of each route.  $k$ -means clustering is then applied to these barycenters to partition the global problem into  $k$  geographically localized subproblems. (ii) *Parallel optimization phase*: For each independent subproblem, an HGS instance is executed in parallel. This enables intensive, localized refinement of the route structures within each cluster, significantly reducing the total computational burden compared to an exhaustive global search. (iii) *Merge phase*: The optimized sub-solutions are re-integrated to form the final high-quality global solution  $S_{\text{expert}}$ .

By leveraging this decomposition-augmented oracle, the training process provides the neural policy with a distribution  $P_E$  that reflects both low-level routing logic and the high-level topological partitioning essential for large-scale optimization.

### 4.4. Adversarial Training Framework

To internalize expert strategies, OD-DEAL employs an adversarial minimax game between the generator  $\pi_\theta$  and a discriminator  $D_\phi$ , transforming sparse terminal rewards into dense feedback via distributional alignment. By minimizing the statistical divergence between the generated distribution  $P_\theta(S)$  and the expert  $P_E(S)$  from HGS-BCC decomposition, the model learns to navigate the solution manifold defined by the decomposition oracle depicted in Figure 1, with further implementation details deferred to Appendix C.

#### 4.4.1. DISCRIMINATOR: EDGE-LEVEL PROBABILISTIC ESTIMATOR

The discriminator  $D_\phi$  is designed as a dense edge-level probability estimator. It shares the GAT-based structural

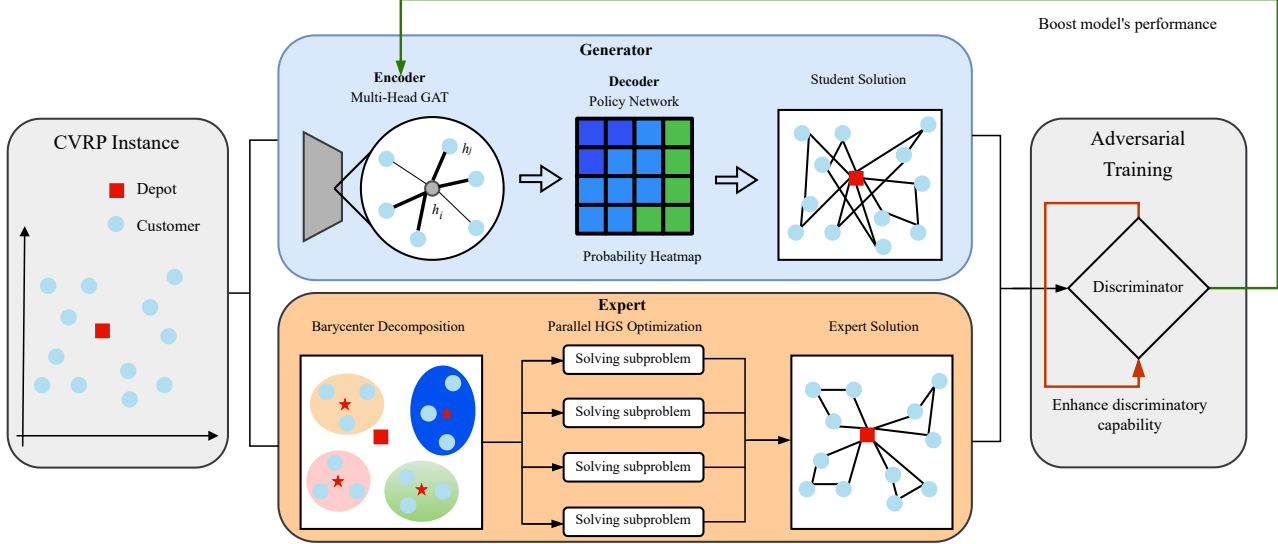


Figure 1. Overall architecture of the OD DEAL framework.

architecture as the generator but serves a distinct evaluative role. Given a CVRP graph  $G = (V, E)$ , The discriminator outputs a comprehensive edge probability matrix  $\mathbf{M}_D \in [0, 1]^{N \times N}$ , where each entry  $\mathbf{M}_{D,ij}$  represents the estimated likelihood that edge  $(i, j)$  belongs to an optimal solution. The discriminator evaluates a candidate solution path  $\tau = \{(v_1, v_2), \dots, (v_k, v_1)\}$  by aggregating the scores of its constituent edges. To align with the generator's objective, we calculate the log-probability score  $D_\phi(\tau)$  as:

$$D_\phi(\tau) = \sum_{(i,j) \in \tau} \log \mathbf{M}_{D,ij}. \quad (9)$$

The dense surrogate reward signal is then derived exponentially:  $R(\tau) = \exp(D_\phi(\tau))$ . This formulation ensures that the reward reflects the joint confidence of all edges in the path. The discriminator is optimized using a least squares GAN objective to distinguish between raw generated policies and their expert-improved counterparts. The training process involves two types of samples. Negative samples ( $\tau_{neg}$ ) are trajectories drawn directly from the generator policy  $\pi_\theta$  without post-processing. The discriminator is optimized to minimize their reward, driving  $R(\tau_{neg}) \rightarrow 0$ . Positive samples ( $\tau_{pos}$ ) are high-quality trajectories obtained by refining generator outputs with the expert policy augmented by BCC decomposition. These trajectories serve as approximations to the target distribution, and the discriminator is trained to maximize their reward, pushing  $R(\tau_{pos}) \rightarrow 1$ . The discriminator loss function is defined as

$$\mathcal{L}_D(\phi) = \mathbb{E}_{\tau_{neg}} [R(\tau_{neg})^2] + \mathbb{E}_{\tau_{pos}} [(1 - R(\tau_{pos}))^2]. \quad (10)$$

During the generator's training phase,  $\pi_\theta$  remains fixed, and only the scalar reward  $R(\tau)$  is used to guide policy updates.

#### 4.4.2. GENERATOR OBJECTIVE AND OPTIMIZATION

The generator  $\pi_\theta$  is optimized to produce solutions that maximize the surrogate reward  $R(\tau)$  provided by the discriminator, effectively aligning the policy with the expert distribution. We define the generator's objective  $J_G(\theta)$  using the trajectory balance (TB) loss from the GFlowNet framework (Bengio et al., 2021a):

$$J_G(\theta) = \mathcal{L}_{TB}(\theta, Z). \quad (11)$$

**Trajectory Balance (TB).** The TB objective to ensures that the generator samples trajectories with a probability proportional to the adversarial reward  $R(\tau) = \exp(D_\phi(\tau))$ . By operating in the log-domain, the loss minimizes the deviation between the parameterized forward flow and the discriminator-guided target:

$$\mathcal{L}_{TB}(\theta, Z) = \mathbb{E}_{\tau \sim \pi_\theta} \left[ \left( \log \frac{Z_\theta P_F(\tau)}{P_B(\tau)} - D_\phi(\tau) \right)^2 \right], \quad (12)$$

where  $Z_\theta$  is a learnable scalar representing the global partition function. Here,  $P_F(\tau)$  denotes the forward trajectory probability, which functions as the energy of the target distribution in the log-domain, guiding the policy toward high-quality regions of the solution space. The backward probability  $P_B(\tau)$  is the product of stepwise backward transitions  $\prod P_B(s_{t-1}|s_t)$ , which represents the probability of returning to a parent state. By incorporating  $P_B(\tau)$ , this loss function enforces flow consistency by ensuring that the forward generative flow  $Z_\theta P_F(\tau)$  matches the backward flow  $P_B(\tau) \exp(D_\phi(\tau))$  guided by the discriminator, satisfying the detailed balance condition and ensuring the correct credit assignment for the solution structure.

**Optimization.** The parameters  $\theta$  and the partition function  $Z_\theta$  are updated via stochastic gradient descent. In each iteration, the gradient  $\mathbf{g}_t$  is computed via backpropagation:

$$\mathbf{g}_t = \nabla_\theta \mathcal{L}_{\text{TB}}(\theta_t). \quad (13)$$

The update rule  $\theta_{t+1} \leftarrow \theta_t - \eta \cdot \mathbf{g}_t$  allows the generator to continuously refine its routing strategy. This GFlowNet-based exploration mechanism allows the model to surpass the initial expert performance. It achieves this by internalizing sophisticated partitioning logic from the dense adversarial feedback provided by the discriminator.

## 5. Experiments

**Dataset Description.** Following established benchmarks (Kwon et al., 2020; Kim et al., 2025), we evaluate OD-DEAL on synthetic CVRP and TSP instances with  $N \in \{200, 500, 1000\}$  nodes for both training and testing. For CVRP instances at other generated scales, the coordinates of both customers and the depot are sampled from a unit square  $[0, 1]^2$ , and customer demands are drawn from  $\text{Unif}\{1, \dots, 9\}$  with vehicle capacity  $Q = 50$ . TSP instances serve as a purely geometric routing baseline. For each scale, the test set contains 128 independent instances, enabling a rigorous assessment of scalability across varying problem sizes.

**Hyperparameters.** For tractability, graphs are sparsified by retaining  $\mathcal{K} = |V|/4$  nearest neighbors per node to preserve critical local topology. During training, the generator performs  $\hat{\mathcal{N}} = 20$  stochastic rollouts to satisfy GFlowNet diversity and exploration. An adversarial update ratio of 4 : 1 between the generator and discriminator is maintained to stabilize the minimax optimization landscape. All baselines use their default parameters. Detailed sensitivity analyses of  $\mathcal{K}$  and  $\hat{\mathcal{N}}$  are provided in the appendix D.2.

**Computational Environment.** All experiments, including the parallel generation of expert solution using HGS-BCC decomposition as well as neural network training, were conducted on a server with an NVIDIA RTX 3090 Ti GPU and an AMD Ryzen Threadripper 3970X 32-core processor. To ensure a fair comparison, all neural baselines were re-trained from scratch under identical hardware and software configurations.

**Performance Metrics.** Performance is evaluated using the mean objective value (Obj.), average inference latency (Time), and optimality gap (%). Optimality gaps are calculated relative to LKH-3 with 100 iterations as the reference baseline. These metrics evaluate the balance between solution quality and computational efficiency, characterizing the model’s performance in large-scale scenarios.

### 5.1. Fixed-Scale Training Comparison

**Baselines:** We evaluate **OD-DEAL-200** (trained solely on 200-node instances) against LKH-3 (Helsgaun, 2000), POMO (Kwon et al., 2020), and NeuOpt (Ma et al., 2024). The upper section of Table 1 reports the generalization performance of these models on test instances with 200, 500, and 1000 nodes. For LKH-3, we report results obtained with 100, 1000, and 10000 iterations. The solution produced by LKH-3 with 100 iterations (i.e., LKH-3 (100)) is used as the uniform benchmark for calculating the optimality gap (%) across all other methods.

**Result:** As illustrated in the **upper half** of Table 1, existing neural baselines suffer from significant performance degradation when generalizing to instances exceeding their training scale. Specifically, while POMO achieves the smallest gap on 200-node instances close to its training distribution, its performance deteriorates drastically as the scale increases. The gaps rise to 18.85% and 45.14% on 500 and 1000 nodes, respectively, with inference time reaching 192.37 seconds for 1000 nodes. NeuOpt generalizes poorly with a 310.58% gap at 500 nodes and failure at 1000 nodes. In contrast, **OD-DEAL-200** demonstrates robust generalization and high inference efficiency. Although its gap on 200-node instances of 5.59% is slightly higher than that of POMO, its relative performance improves markedly as problem scale increases. The gap decreases to 1.71% for 500-node instances and reaches -2.76% for 1000-node instances, achieving an objective value of 128.13 versus 131.77 for LKH-3(100). These results indicate that a model trained solely on 200-node instances not only avoids performance collapse at larger scales but also surpasses the LKH-3(100) benchmark. OD-DEAL-200 sustains subsecond inference across all scales. At 1000 nodes, it is approximately **300 times faster (0.66 s vs. 192.37 s)** than POMO and three times faster than LKH-3(100) (2.14 s). Although GLOP is faster, its gap reaches 19.55%. In contrast, OD-DEAL-200 achieves a superior balance, yielding a negative optimality gap (-2.76%) in sub-second inference (0.66 s).

### 5.2. Scalability Analysis across Training Scales

**Baselines:** For evaluations across different training scales, we include the heuristic ACO (Mazzeo & Loiseau, 2004) and GFACS (Kim et al., 2025), which integrates GFlowNet with ACO. We provide results for both AGFN and OD-DEAL trained on instances with 200, 500, and 1000 nodes. To isolate generative performance, no methods utilize local search or refinement after construction.

**Result:** Results in the **lower half** of Table 1 demonstrate that OD-DEAL consistently achieves the superior trade-off between solution quality and inference efficiency. Every variant maintains subsecond runtimes across all problem scales. In particular, OD-DEAL-500 attains the best perfor-

Table 1. Overall performance comparison on the synthetic CVRP dataset. The *Obj.* denotes the average total travel distance, while *Time* indicates the average time to solve per instance. The best results are highlighted in bold and the second-best results are indicated with underlining.

| METHOD       | OBJ.             | $ V  = 200$  |             | TIME (S)         | $ V  = 500$  |             | TIME (S)          | $ V  = 1000$ |             | TIME (S) |
|--------------|------------------|--------------|-------------|------------------|--------------|-------------|-------------------|--------------|-------------|----------|
|              |                  | GAP (%)      | TIME (S)    |                  | GAP (%)      | TIME (S)    |                   | GAP (%)      | TIME (S)    |          |
| LKH-3(100)   | 28.816896        | —            | 0.47        | 66.812744        | —            | 1.06        | 131.771685        | —            | 2.14        |          |
| LKH-3(1000)  | 28.213308        | -2.09        | 4.30        | 64.147637        | -3.99        | 8.46        | 123.169293        | -6.53        | 15.19       |          |
| LKH-3(10000) | 28.024617        | -2.75        | 44.58       | 63.320593        | -5.23        | 84.31       | 120.260032        | -8.74        | 141.04      |          |
| POMO         | <b>29.141700</b> | <b>1.13</b>  | 2.60        | 79.408600        | 18.85        | 24.09       | 191.255300        | 45.14        | 192.37      |          |
| NEUOPT       | <u>29.459557</u> | <u>2.23</u>  | 1.24        | 274.321472       | 310.58       | 3.74        | —                 | —            | —           |          |
| GLOP         | 33.779831        | 17.22        | 0.20        | <u>77.640152</u> | <u>16.21</u> | <b>0.27</b> | 157.538406        | 19.55        | <b>0.39</b> |          |
| OD-DEAL-200  | 30.426691        | 5.59         | <b>0.13</b> | <b>67.955727</b> | <u>1.71</u>  | <u>0.32</u> | <u>128.135544</u> | <u>-2.76</u> | 0.66        |          |
| ACO          | 97.195656        | 237.29       | 1.32        | 248.330895       | 271.68       | 7.25        | 503.110024        | 281.80       | 26.97       |          |
| GFACS        | <b>28.507015</b> | <b>-1.08</b> | 3.25        | <b>64.381401</b> | <b>-3.64</b> | 8.22        | <b>122.071861</b> | <b>-7.36</b> | 15.82       |          |
| AGFN-200     | 30.680285        | 6.47         | 0.14        | 69.596748        | 4.17         | 0.33        | 132.565826        | 0.60         | 0.68        |          |
| AGFN-500     | 32.240875        | 11.88        | 0.14        | 69.417389        | 3.90         | 0.33        | 128.989380        | -2.11        | 0.68        |          |
| AGFN-1000    | 32.677258        | 13.40        | 0.14        | 70.010994        | 4.79         | 0.33        | 129.627396        | -1.63        | 0.69        |          |
| OD-DEAL-200  | <u>30.426691</u> | <u>5.59</u>  | <u>0.13</u> | 67.955727        | 1.71         | <b>0.32</b> | 128.135544        | -2.76        | 0.66        |          |
| OD-DEAL-500  | <u>31.745686</u> | <u>10.16</u> | <u>0.13</u> | <u>67.915985</u> | <u>1.65</u>  | <u>0.32</u> | <u>126.895134</u> | <u>-3.70</u> | <b>0.65</b> |          |
| OD-DEAL-1000 | 33.813118        | 17.34        | <u>0.13</u> | 68.957115        | 3.21         | <u>0.32</u> | 127.634361        | -3.14        | 0.66        |          |

formance on 1000-node instances, achieving a  $-3.70\%$  optimality gap in just 0.65 seconds. At matched training scales, OD-DEAL consistently outperforms AGFN in both optimality gap and speed. For instance, OD-DEAL-500 reduces the optimality gap on 500-node instances from  $3.90\%$  to  $1.65\%$ , and further improves performance on 1,000-node instances from  $-2.11\%$  to  $-3.70\%$ , while also achieving slightly faster inference (0.32 s vs. 0.33 s). Against ACO, OD-DEAL-500 reduces runtime by over 97% while providing significantly better solutions. Although GFACS yields lower gaps (e.g.,  $-7.36\%$  at 1,000 nodes), it incurs approximately 24 times more inference latency. These findings confirm that OD-DEAL provides highly accurate solutions with instantaneous speed for large-scale CVRP.

The experimental results validate our adversarial distillation paradigm. Table 1 shows that at  $N = 1000$ , baselines like POMO and NeuOpt degrade significantly, with optimality gaps exceeding 45%, confirming that sparse rewards fail in massive search spaces. OD-DEAL consistently maintains low optimality gaps across all scales due to the discriminator induced target distribution that provides dense gradient signals beyond simple scalar rewards. OD-DEAL achieves inference speeds multiple orders of magnitude faster than traditional heuristics. These results demonstrate that the GAT generator internalizes expert decomposition and search strategies, yielding an effective balance between solution quality and inference efficiency for instantaneous routing.

### 5.3. Generalization Analysis

To evaluate robustness across distributions and ultra-large-scale scenarios, we applied OD-DEAL-200 model, trained exclusively on synthetic instances with 200 nodes, to real world benchmarks and synthetic instances with up to 10000 nodes. These evaluations involve CVRPLib (Augerat et al., 1995; Christofides, 1979; Rochat & Taillard, 1995),

TSPLib (Reinelt, 1995), and the latest released CVRPLib-XL datasets (Queiroga et al., 2026). Further results are provided in Appendix D.3.

**Inference on Real World Datasets.** Table 2 illustrates the performance of different models on the CVRPLib and TSPLib benchmarks. The results demonstrate that while solvers exhibit various balances of quality and efficiency, OD-DEAL provides the superior overall performance across these real world instances.

*Trade-off between Solution Quality and Efficiency:* OD-DEAL outperforms other end-to-end generative models. CVRPLib evaluations yield an average objective value of 133463 for OD-DEAL-200. This result represents a substantial improvement over AGFN-200 (187079.20) and GLOP-1000 (217283.90). GFACS attains a lower objective value of 112042.50. GFACS performance gains require disproportionately higher computational overhead.

*Superiority in Inference Speed:* OD-DEAL exhibits a significant efficiency advantage in inference efficiency. CVRPLib evaluations yield a 39-second average runtime for OD-DEAL-200. GLOP-1000 necessitates 63.62 seconds. GFACS-200 requires 131.39 seconds. OD-DEAL-200 achieves a 3.3-fold speed advantage. TSPLib results demonstrate widened performance gaps. GFACS-200 requires 168.44 seconds. OD-DEAL-200 necessitates 45.73 seconds. These results indicate that OD-DEAL delivers high quality solutions with substantially lower latency, making it suitable for real time logistics applications.

**Scalability on Ultra-Large-Scale Instances.** Table 3 reports performance on ultra-large-scale CVRP instances, highlighting OD-DEAL’s advantages in handling complex, large-scale problems. On 2000-node instances, OD-DEAL-200 achieves an average path length of 244.41, close to LKH-3 (1,000 iterations) at 243.57, with 3.06 seconds for

Table 2. Overall performance comparison on CVRPLib and TSPLib datasets. The *Obj.* indicates the total travel distance, while *Time* denotes the total time to solve all instances.

| CVRPLib  | Optimal   | OD-DEAL-200  | AGFN-200  | GFACS-200        | GLOP-1000 | TSPLib   | Optimal    | OD-DEAL-200 | AGFN-200     | GFACS-200  | GLOP-1000         |
|----------|-----------|--------------|-----------|------------------|-----------|----------|------------|-------------|--------------|------------|-------------------|
| Obj.     | 110261.63 | 133463.00    | 187079.20 | <b>112042.50</b> | 217283.90 | Obj.     | 769.953827 | 987.702364  | 915.542687   | 807.992956 | <b>788.482424</b> |
| Time (s) | -         | <b>39.00</b> | 39.05     | 131.39           | 63.62     | Time (s) | -          | 45.73       | <b>42.90</b> | 168.44     | 680.62            |
| Gap (%)  | -         | 21.04        | 69.67     | <b>1.62</b>      | 97.06     | Gap (%)  | -          | 28.28       | 18.91        | 5.72       | <b>2.41</b>       |

Table 3. Comparative results on ultra-large-scale synthetic CVRP datasets with up to 10000 nodes. The *Obj.* indicates the average total travel distance, while *Time* denotes the average time to solve a single instance.

| CVRP        | OBJ.              | V  = 2000 |             | TIME (S)          | OBJ. | V  = 5000   |                    | TIME (S) | OBJ.        | V  = 10000 |          |
|-------------|-------------------|-----------|-------------|-------------------|------|-------------|--------------------|----------|-------------|------------|----------|
|             |                   | GAP (%)   | TIME (S)    |                   |      | GAP (%)     | TIME (S)           |          |             | GAP (%)    | TIME (S) |
| LKH-3(1000) | 243.569497        | -         | 28.49       | 631.602489        | -    | 47          | 1292.649936        | -        | 65.85       |            |          |
| AGFN-200    | 254.051392        | -         | 7.55        | 587.557190        | -    | 19.53       | 1145.796509        | -        | 38.36       |            |          |
| OD-DEAL-200 | 244.406403        | -         | 3.06        | 584.840210        | -    | 9.46        | 1177.169800        | -        | 12.1        |            |          |
| GFACS-200   | <b>236.277512</b> | -         | 5.56        | <b>563.053345</b> | -    | 23.33       | <b>1106.582520</b> | -        | 42.42       |            |          |
| GLOP        | 287.393829        | -         | <b>1.01</b> | 712.800415        | -    | <b>1.76</b> | 1319.468384        | -        | <b>3.94</b> |            |          |
| POMO-100    | 648.761200        | -         | 3.35        | 2146.482600       | -    | 76.47       | -                  | -        | -           | -          | -        |

inference. This runtime is faster than POMO-100 (3.35 s). GLOP completes in 1.01 seconds but has worse solution quality (287.39). GFACS-200 attains a slightly lower objective (236.28) but requires 5.56 seconds.

As the scale increases to 5000 nodes, OD-DEAL completes inference in 9.46 seconds and achieves superior performance compared with AGFN-200 (19.53 s, Obj. 587.56) and POMO-100 (Obj. 2146.48, 76.47 s). GFACS provides slightly better objective (563.05) with 23.33 seconds runtime. GLOP remains fast (1.76 s) but exhibits larger optimality gap (712.80).

The 10000-node scenario highlights OD-DEAL efficiency gains. POMO fails to generate valid solutions at this scale. OD-DEAL produces an objective value of 1177.17 in 12.1 seconds. LKH-3 yields an objective of 1292.65 under equivalent runtime constraints. AGFN (1145.80) and GFACS (1106.58) provide reasonable solution quality. Respective inference times (38.36s and 42.42s) exceed OD-DEAL latency by over 300%. GLOP achieves a 3.94-second inference time. GLOP yields the least accurate solution (1319.47). Extreme-scale constraints reveal critical performance limitations in baseline architectures. The accuracy-latency equilibrium validates framework generalization. Dynamic expert-guided mechanisms demonstrate efficacy for ultra-large-scale CVRP.

#### 5.4. Ablation Study

We evaluate OD-DEAL against two variants: *noCluster*, which excludes expert clustering, and *Transformer*, which replaces the GAT backbone. Detailed results for these ablation experiments are provided in Appendix D.1.

**Impact of Clustering Optimization.** On CVRP instances, OD-DEAL-noCluster consistently yields higher optimality gaps and longer runtimes across all training size groups. At 500 nodes, the gap increases from 1.65% to 2.74%, and

runtime rises from 0.32 to 0.54 seconds. For TSP instances, removing clustering improves solution quality but requires more computation time. At 1000 nodes, the gap reaches 8.86% compared to 19.32%, while time increases from 0.16 to 0.17 seconds.

**Architectural Comparison.** Replacing the GAT with a Transformer reduces CVRP performance significantly across all problem scales. For 500 nodes, the gap expands from 1.65% to 4.92%. Conversely, the Transformer variant achieves lower gaps on TSP tasks than the original model within each training group. At 500 nodes, the gap improves from 12.66% to 10.23%.

**Discussion.** These results confirm the importance of expert-guided decomposition for large-scale CVRP, as BCC-based decomposition provides high-quality reference signals that direct HGS optimization cannot reliably achieve. The results also demonstrate the advantage of GAT encoders over Transformers in modeling nonlinear spatial and demand-dependent interactions. Overall, the findings indicate that expert clustering and specialized architectural backbones are essential for high-quality route construction.

## 6. Conclusion

This paper proposed OD-DEAL, an adversarial learning framework that addresses neural scalability bottlenecks in large-scale CVRP. By distilling “divide-and-conquer” logic from an HGS-BCC expert into a generative GAT policy, OD-DEAL enables high-quality, clustering-free inference on massive graphs. Empirical results show that OD-DEAL sets a new real-time SOTA, achieving near-constant neural scaling and sub-second inference on instances of up to 10000 nodes. This paradigm effectively bridges the gap between expert heuristics and scalable neural optimization. Future work will extend this framework to multi-constraint variants like CVRP with time windows and refine its inductive bi-

ases for homogeneous graph structures. The limitations of OD-DEAL are discussed in Appendix F.

## Impact Statement

This paper presents work whose goal is to advance the field of Machine Learning. There are many potential societal consequences of our work, none which we feel must be specifically highlighted here.

## References

Augerat, P., Naddef, D., Belenguer, J., Benavent, E., Corberan, A., and Rinaldi, G. Computational results with a branch and cut code for the capacitated vehicle routing problem, 1995. Technical report.

Bello, I., Pham, H., Le, Q. V., Norouzi, M., and Bengio, S. Neural combinatorial optimization with reinforcement learning. In *5th International Conference on Learning Representations Workshop Track*, 2017.

Bengio, E., Jain, M., Korablyov, M., Precup, D., and Bengio, Y. Flow network based generative models for non-iterative diverse candidate generation. *Advances in Neural Information Processing Systems*, 34:27381–27394, 2021a.

Bengio, Y., Lodi, A., and Prouvost, A. Machine learning for combinatorial optimization: a methodological tour d’horizon. *European Journal of Operational Research*, 290(2):405–421, 2021b.

Bengio, Y., Lahlou, S., Deleu, T., Hu, E. J., Tiwari, M., and Bengio, E. Gflownet foundations. *Journal of Machine Learning Research*, 24(210):1–55, 2023.

Bi, J., Ma, Y., Wang, J., Cao, Z., Chen, J., Sun, Y., and Chee, Y. M. Learning generalizable models for vehicle routing problems via knowledge distillation. *Advances in Neural Information Processing Systems*, 35:31226–31238, 2022.

Bogyrbayeva, A., Meraliyev, M., Mustakhov, T., and Dauletbayev, B. Machine learning to solve vehicle routing problems: A survey. *IEEE Transactions on Intelligent Transportation Systems*, 25(6):4754–4772, 2024.

Bui, V. and Mai, T. Imitation improvement learning for large-scale capacitated vehicle routing problems. In *Proceedings of the International Conference on Automated Planning and Scheduling*, volume 33, pp. 551–559, 2023.

Cappart, Q., Chételat, D., Khalil, E. B., Lodi, A., Morris, C., and Veličković, P. Combinatorial optimization and reasoning with graph neural networks. *Journal of Machine Learning Research*, 24(130):1–61, 2023.

Christofides, N. The vehicle routing problem. *Combinatorial optimization*, 1979.

Gunarathna, U., Borovica-Gajic, R., Karunasekera, S., and Tanin, E. Dynamic graph combinatorial optimization with multi-attention deep reinforcement learning. In *Proceedings of the 30th International Conference on Advances in Geographic Information Systems*, pp. 1–12, 2022.

Helsgaun, K. An effective implementation of the lin-kernighan traveling salesman heuristic. *European Journal of Operational Research*, 126(1):106–130, 2000.

Helsgaun, K. An extension of the lin-kernighan-helsgaun TSP solver for constrained traveling salesman and vehicle routing problems. *Roskilde: Roskilde University*, 12:966–980, 2017.

Jiao, D., Wang, L., Yang, P., Yang, W., Peng, Y., Shang, Z., and Ren, F. Unmanned aerial vehicle-enabled grassland restoration with energy-sensitive of trajectory design and restoration areas allocation via a cooperative memetic algorithm. *Engineering Applications of Artificial Intelligence*, 133:108084, 2024.

Kerscher, C. and Minner, S. Decompose-route-improve framework for solving large-scale vehicle routing problems with time windows. *Transportation Research Part E: Logistics and Transportation Review*, 204:104409, 2025.

Kim, H., Kim, M., Choi, S., and Park, J. Genetic-guided gflownets: Advancing in practical molecular optimization benchmark. *Advances in Neural Information Processing Systems*, 2024.

Kim, M., Choi, S., Kim, H., Son, J., Park, J., and Bengio, Y. Ant colony sampling with gflownets for combinatorial optimization. In *International Conference on Artificial Intelligence and Statistics*, pp. 469–477, 2025.

Kool, W., van Hoof, H., and Welling, M. Attention, learn to solve routing problems! In *International Conference on Learning Representations*, 2019.

Kotary, J., Fioretto, F., Van Hentenryck, P., and Wilder, B. End-to-end constrained optimization learning: A survey. In *International Joint Conference on Artificial Intelligence*, pp. 4475–4482, 2021. Survey Track.

Kwon, Y.-D., Choo, J., Kim, B., Yoon, I., Gwon, Y., and Min, S. Pomo: Policy optimization with multiple optima for reinforcement learning. *Advances in Neural Information Processing Systems*, 33:21188–21198, 2020.

Laporte, G. Fifty years of operational research: 1972–2022. *European Journal of Operational Research*, 319(2):347–360, 2024.

Liu, S., Tang, K., and Yao, X. Memetic search for vehicle routing with simultaneous pickup-delivery and time windows. *Swarm and Evolutionary Computation*, 66:100927, 2021.

Liu, S., Zhang, Y., Tang, K., and Yao, X. How good is neural combinatorial optimization? a systematic evaluation on the traveling salesman problem. *IEEE Computational Intelligence Magazine*, 18(3):14–28, 2023.

Luo, F., Lin, X., Liu, F., Zhang, Q., and Wang, Z. Neural combinatorial optimization with heavy decoder: Toward large scale generalization. *Advances in Neural Information Processing Systems*, 36:8845–8864, 2023.

Luo, F., Lin, X., Wu, Y., Wang, Z., Xialiang, T., Yuan, M., and Zhang, Q. Boosting neural combinatorial optimization for large-scale vehicle routing problems. In *The Thirteenth International Conference on Learning Representations*, 2025.

Ma, Y., Cao, Z., and Chee, Y. M. Learning to search feasible and infeasible regions of routing problems with flexible neural k-opt. *Advances in Neural Information Processing Systems*, 36, 2024.

Mazzeo, S. and Loiseau, I. An ant colony algorithm for the capacitated vehicle routing. *Electronic Notes in Discrete Mathematics*, 18:181–186, 2004.

Queiroga, E., Martinelli, R., Subramanian, A., Uchoa, E., and Vidal, T. The XL instances for the capacitated vehicle routing problem. *arXiv preprint arXiv:2601.11467*, 2026.

Reinelt, G. Tsplib95. *Interdisziplinäres Zentrum für Wissenschaftliches Rechnen (IWR), Heidelberg*, 338:1–16, 1995.

Rochat, Y. and Taillard, É. D. Probabilistic diversification and intensification in local search for vehicle routing. *Journal of Heuristics*, 1(1):147–167, 1995.

Santini, A., Schneider, M., Vidal, T., and Vigo, D. Decomposition strategies for vehicle routing heuristics. *INFORMS Journal on Computing*, 35(3):543–559, 2023.

Sun, Z. and Yang, Y. Difusco: Graph-based diffusion solvers for combinatorial optimization. *Advances in Neural Information Processing Systems*, 36:3706–3731, 2023.

Toth, P. and Vigo, D. *Vehicle routing: problems, methods, and applications*. SIAM, 2014.

Veličković, P., Cucurull, G., Casanova, A., Romero, A., Lio, P., and Bengio, Y. Graph attention networks. In *International Conference on Learning Representations*, 2018.

Vidal, T. Hybrid genetic search for the CVRP: Open-source implementation and swap\* neighborhood. *Computers & Operations Research*, 140:105643, 2022.

Vidal, T., Crainic, T. G., Gendreau, M., Lahrichi, N., and Rei, W. A hybrid genetic algorithm for multidepot and periodic vehicle routing problems. *Operations Research*, 60(3):611–624, 2012.

Williams, R. J. Simple statistical gradient-following algorithms for connectionist reinforcement learning. *Machine learning*, 8(3):229–256, 1992.

Wu, X., Wang, D., Wen, L., Xiao, Y., Wu, C., Wu, Y., Yu, C., Maskell, D. L., and Zhou, Y. Neural combinatorial optimization algorithms for solving vehicle routing problems: A comprehensive survey with perspectives. *arXiv preprint arXiv:2406.00415*, 2024.

Xu, R., Fan, X., Liu, S., Chen, W., and Tang, K. Memetic search for green vehicle routing problem with private capacitated refueling stations. *IEEE Transactions on Evolutionary Computation*, 2025. doi: 10.1109/TEVC.2025.3639252.

Yao, S., Lin, X., Wang, J., Zhang, Q., and Wang, Z. Rethinking supervised learning-based neural combinatorial optimization for routing problem. *ACM Transactions on Evolutionary Learning*, 5(4):1–24, 2025.

Ye, H., Wang, J., Liang, H., Cao, Z., Li, Y., and Li, F. Glop: Learning global partition and local construction for solving large-scale routing problems in real-time. In *Proceedings of the AAAI conference on Artificial Intelligence*, volume 38, pp. 20284–20292, 2024.

Zhang, D., Dai, H., Malkin, N., Courville, A. C., Bengio, Y., and Pan, L. Let the flows tell: Solving graph combinatorial problems with gflownets. *Advances in Neural Information Processing Systems*, 36:11952–11969, 2023.

Zhang, N. and Cao, Z. Hybrid-balance gflownet for solving vehicle routing problems. In *The Thirty-ninth Annual Conference on Neural Information Processing Systems*, 2025.

Zhang, N., Yang, J., Cao, Z., and Chi, X. Adversarial generative flow network for solving vehicle routing problems. In *The Thirteenth International Conference on Learning Representations*, 2025.

Zheng, Z., Yao, S., Wang, Z., Tong, X., Yuan, M., and Tang, K. DPN: decoupling partition and navigation for neural solvers of min-max vehicle routing problems. In *Proceedings of the 41st International Conference on Machine Learning*, pp. 61559–61592, 2024a.

Zheng, Z., Zhou, C., Xialiang, T., Yuan, M., and Wang, Z. Udc: A unified neural divide-and-conquer framework for large-scale combinatorial optimization problems. *Advances in Neural Information Processing Systems*, 37: 6081–6125, 2024b.

Zheng, Z., Liu, S., and Ong, Y.-S. Hybrid memetic search for electric vehicle routing with time windows, simultaneous pickup-delivery, and partial recharges. *IEEE Transactions on Emerging Topics in Computational Intelligence*, 9(3):3773–3787, 2025.

Zong, Z., Wang, H., Wang, J., Zheng, M., and Li, Y. Rbg: Hierarchically solving large-scale routing problems in logistic systems via reinforcement learning. In *Proceedings of the 28th ACM SIGKDD Conference on Knowledge Discovery and Data Mining*, pp. 4648–4658, 2022.

## A. Formal Mathematical Formulations

### A.1. Mathematical Formulation for the CVRP

The capacitated vehicle routing problem (CVRP) is a fundamental challenge in combinatorial optimization. This section provides a formal integer linear programming (ILP) formulation. The objective is to design optimal delivery routes that minimize total travel cost while satisfying vehicle capacity constraints. Following the classical flow-based formulation, we define the problem on a graph  $G(V, E)$ , where  $V = \{v_0\} \cup V_c$  represents the depot and the set of customers, respectively. We introduce binary decision variables  $x_{ij} \in \{0, 1\}$ , where  $x_{ij} = 1$  if a vehicle traverses the edge from node  $i$  to node  $j$ , and 0 otherwise. Meanwhile, a continuous variable  $u_i$  represents the cumulative load upon arrival at node  $i$ , serving to both enforce capacity limits and eliminate subtours. The CVRP is formulated as follows:

$$\min \sum_{i \in V} \sum_{\substack{j \in V \\ j \neq i}} c_{ij} x_{ij} \quad (14a)$$

$$\text{s.t. } \sum_{\substack{j \in V \\ j \neq i}} x_{ij} = 1, \quad \forall i \in V_c, \quad (14b)$$

$$\sum_{\substack{i \in V \\ i \neq j}} x_{ij} - \sum_{\substack{k \in V \\ k \neq j}} x_{jk} = 0, \quad \forall j \in V_c, \quad (14c)$$

$$\sum_{j \in V_c} x_{0j} \leq K, \quad (14d)$$

$$u_i - u_j + Qx_{ij} \leq Q - d_j, \quad \forall i, j \in V_c, i \neq j, \quad (14e)$$

$$d_i \leq u_i \leq Q, \quad \forall i \in V_c, \quad (14f)$$

$$x_{ij} \in \{0, 1\}, \quad \forall i, j \in V, i \neq j, \quad (14g)$$

$$u_i \geq 0, \quad \forall i \in V_c. \quad (14h)$$

The objective function (14a) minimizes the total travel cost (e.g., total distance or time) for the entire fleet. constraints (14b) and (14c) enforce service uniqueness and flow conservation, ensuring that each customer is visited exactly once and that vehicles maintain path continuity. Constraints (14d) restrict the total number of vehicles departing from the depot not to exceed the fleet size  $K$ . To prevent the formation of isolated subtours and enforce the vehicle capacity  $Q$ , we utilize the Miller-Tucker-Zemlin (MTZ) formulation in (14e), where the auxiliary variables  $u_i$  track the cumulative demand along each route. Finally, constraints (14f)-(14h) define the binary requirements for the routing variables and the feasible ranges for the continuous load variables, ensuring a rigorous mathematical representation of the problem.

### A.2. Mathematical Formulation for the TSP

The traveling salesman problem (TSP) is a foundational task in combinatorial optimization and can be viewed as a specialized case of the CVRP. In this section, we provide a formal integer linear programming (ILP) formulation of the TSP to establish the theoretical basis for our subsequent experimental analysis.

The objective of the TSP is to identify the minimum-cost Hamiltonian cycle that visits each node in a set  $V = \{1, \dots, n\}$  exactly once before returning to the origin. Formally, let  $G = (V, E)$  be a complete graph where  $c_{ij}$  represents the cost associated with edge  $(i, j) \in E$ . We define the binary decision variable  $x_{ij} \in \{0, 1\}$ , which equals 1 if the path traverses directly from node  $i$  to node  $j$ , and 0 otherwise. To prevent the formation of isolated subtours, we employ the Miller-Tucker-Zemlin (MTZ) formulation, introducing auxiliary continuous variables  $u_i$  to track the sequence of visitation. The TSP is formulated as follows:

$$\min \sum_{i \in V} \sum_{\substack{j \in V \\ j \neq i}} c_{ij} x_{ij} \quad (15a)$$

$$\text{s.t. } \sum_{\substack{j \in V \\ j \neq i}} x_{ij} = 1, \quad \forall i \in V, \quad (15b)$$

$$\sum_{\substack{i \in V \\ i \neq j}} x_{ij} = 1, \quad \forall j \in V, \quad (15c)$$

$$u_i - u_j + nx_{ij} \leq n - 1, \forall i, j \in \{2, \dots, n\}, i \neq j, \quad (15d)$$

$$1 \leq u_i \leq n - 1, \quad \forall i \in \{2, \dots, n\}, \quad (15e)$$

$$x_{ij} \in \{0, 1\}, \quad \forall i, j \in V, i \neq j. \quad (15f)$$

The objective function (15a) minimizes the total travel cost of the Hamiltonian cycle. Constraints (15b) and (15c) are the degree constraints, which respectively ensure that exactly one edge departs from and enters every node; together, they guarantee that each city is visited exactly once. Constraints (15d) denote the Miller-Tucker-Zemlin (MTZ) subtour elimination criteria. It enforces that if a path exists from  $i$  to  $j$  (i.e.,  $x_{ij} = 1$ ), then the visitation order must satisfy  $u_j \geq u_i + 1$ . These constraints preclude the formation of closed loops (subtours) that do not include the designated starting node (node 1). Finally, constraints (15e) and (15f) define the feasible domains for the auxiliary sequence variables  $u_i$  and the binary decision variables  $x_{ij}$ .

## B. Graph Attention Network (GAT) Encoder

In the OD-DEAL framework, the generator adopts a graph attention networks (GAT) as its core policy architecture. GATs are particularly well-suited to the CVRP because they overcome the limitations of standard graph convolutional networks (GCNs). In particular, GATs dynamically weight interactions among customer nodes through an attention mechanism, enabling the model to capture heterogeneous node features and adapt to varying graph topologies. These properties are critical for routing problems, where long-range spatial dependencies and demand heterogeneity play a central role. This section introduces the construction of input features, presents the mathematical formulation of the attention mechanism, and describes the multi-head attention aggregation strategy.

For a given CVRP instance, the input to the GAT is a node feature matrix  $X = \{\mathbf{x}_1, \mathbf{x}_2, \dots, \mathbf{x}_N\}$ , where each  $\mathbf{x}_i \in \mathbb{R}^F$  represents the raw feature vector of node  $i$ . In our implementation,  $\mathbf{x}_i$  contains the normalized 2D coordinates  $(x_i, y_i)$  and the customer demand  $d_i$ . To project these features into a high-dimensional representation space, we apply a learnable linear transformation via a shared weight matrix  $W_{node} \in \mathbb{R}^{D_{units} \times F}$ . The initial hidden state  $\mathbf{h}_i^{(0)} = \sigma(W_{node}\mathbf{x}_i + b_{node})$ . This projection maps raw inputs into a unified latent space. It enables the model to capture complex spatial and demand-based relationships between nodes in subsequent attention layers.

The primary innovation of GAT is its self-attention mechanism, which enables nodes to dynamically assign aggregation weights based on neighborhood features, rather than relying on a fixed graph Laplacian matrix. Following Veličković et al. (Veličković et al., 2018), for a node  $i$  and its neighbor  $j \in \mathcal{N}_i$ , the attention coefficient  $s_{ij}$  quantifies the relative importance of node  $j$  to node  $i$ . This paper adopts an additive attention mechanism:

$$s_{ij} = \text{LeakyReLU}(\vec{a}^T [W_{node}\mathbf{x}_i || W_{node}\mathbf{x}_j]), \quad (16)$$

where  $||$  denotes the vector concatenation operation and  $\vec{a} \in \mathbb{R}^{2D_{units}}$  is a learnable weight vector of a single-layer feedforward neural network. To normalize these coefficients into a probability distribution, we apply the softmax function:  $\alpha_{ij} = \text{softmax}_j(s_{ij})$ . This weight  $\alpha_{ij}$  explicitly dictates the contribution of node  $j$ 's feature during the information passing process to node  $i$ .

To stabilize training and capture diverse feature subspaces, such as geographic proximity or demand-capacity correlations, we utilize a multi-head attention mechanism. With  $K$  independent attention heads, the intermediate layers employ a concatenation strategy:  $\mathbf{h}'_i = \|\sum_{k=1}^K \sigma(\sum_{j \in \mathcal{N}_i} \alpha_{ij}^k W^k \mathbf{x}_j)\|$ . For the output layer, an averaging strategy is used to produce a fixed-dimension embedding. Compared to fully connected Transformer-based architectures with  $O(N^2)$  complexity, GAT offers significant advantages for large-scale CVRP. By restricting attention to a  $k$ -nearest neighbor ( $k$ -NN) graph, the complexity is reduced to  $O(kN)$ , drastically improving inference speed. Furthermore, the explicit modeling of graph topology provides GAT with strong permutation invariance, a fundamental property for routing problems where solution quality must be independent of node indexing.

## C. OD-DEAL Framework Design and Workflow

### C.1. Procedural Workflow

As illustrated in Figure 2, we propose OD-DEAL, an expert-guided adversarial learning framework that utilizes online decomposition to solve large-scale CVRP. The architecture consists of three primary modules: a GAT-based generator serving as the neural routing policy, a hybrid expert standard that leverages barycenter clustering (BCC) decomposition-augmented hybrid genetic search (HGS), and an adversarial discriminator designed to facilitate high-fidelity knowledge distillation.

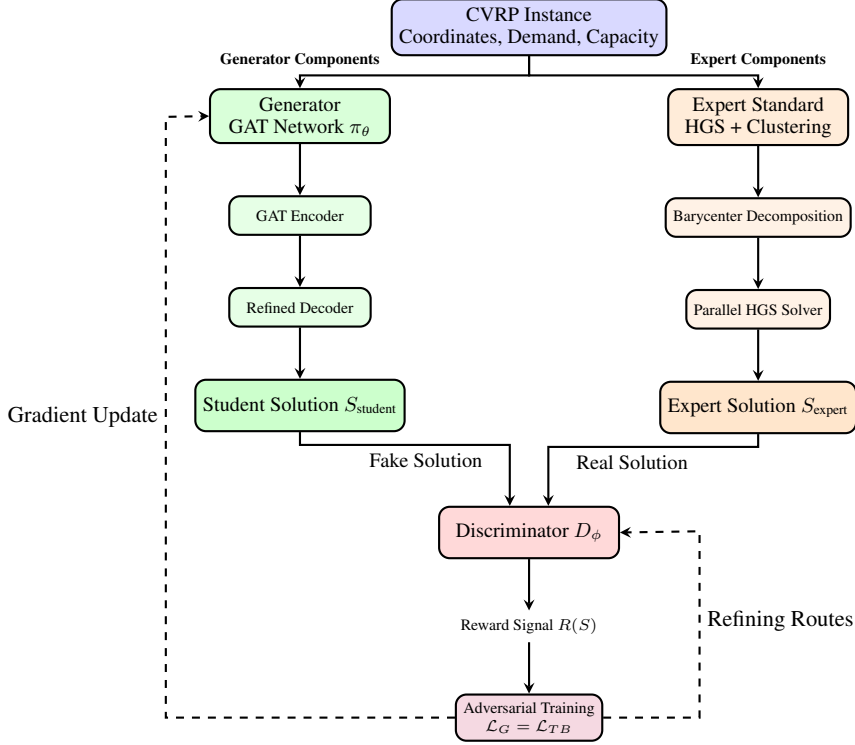


Figure 2. Procedural workflow of the OD-DEAL framework.

### C.2. Parallel Decomposition and Expert Interaction

The operational workflow of OD-DEAL proceeds as follows. (i) **Input.** The framework receives a CVRP instance, including node coordinates, customer demands, and vehicle capacity constraints. (ii) **Generator Solving.** The generator  $\pi_\theta$ , implemented as a GAT-based policy network, processes the instance and produces a candidate solution  $S_{\text{student}}$ . (iii) **Expert Standard Generation.** An expert solver based on HGS, augmented with online BCC, solves the same instance to obtain a high-quality reference solution  $S_{\text{expert}}$  in real-time. (iv) **Discriminator Evaluation.** The discriminator  $D_\phi$  evaluates solutions from both the generator and the expert, estimating the probability that a given solution belongs to the high-quality solution distribution. (v) **Adversarial Training.** Through a dynamic minimax optimization scheme, the discriminator learns to differentiate between  $S_{\text{student}}$  from  $S_{\text{expert}}$ , while the generator minimizes a combined adversarial loss. This interaction drives the generator to explore the solution space and internalize the expert’s “divide-and-conquer” partitioning rules, effectively aligning its output distribution with that of the high-quality expert oracle. (vi) **Inference.** After training, the framework bypasses the expert and discriminator components, utilizing only the neural policy  $\pi_\theta$  for rapid, clustering-free inference on large-scale routing instances.

## D. Extended Experimental Results

### D.1. Comprehensive Ablation Studies

To evaluate the significance of each core component, we conduct extensive ablation experiments, with results summarized in Figures 3 and 4, and detailed performance metrics reported in Table 4.

## Part I: CVRP Results

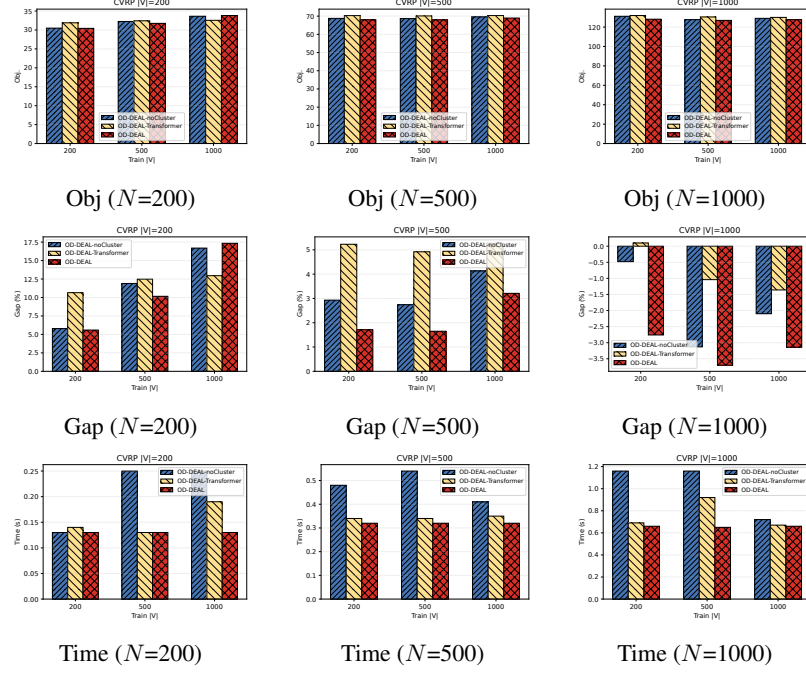


Figure 3. Ablation study results on CVRP.

## Part II: TSP Results

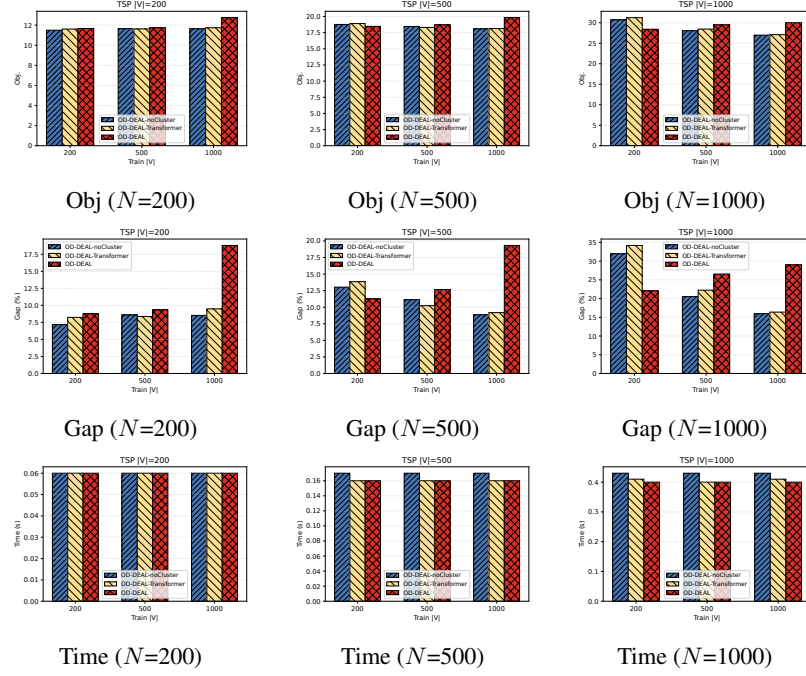


Figure 4. Ablation study results on TSP.

Table 4. Ablation study comparing OD-DEAL with no-clustering and Transformer variants on CVRP and TSP.

| CVRP Method              | Obj.             | $ V  = 200$<br>Gap (%) | Time (s)    | Obj.             | $ V  = 500$<br>Gap (%) | Time (s)    | Obj.              | $ V  = 1000$<br>Gap (%) | Time (s)    | TSP Method               | Obj.             | $ V  = 200$<br>Gap (%) | Time (s)    | Obj.             | $ V  = 500$<br>Gap (%) | Time (s)    | Obj.             | $ V  = 1000$<br>Gap (%) | Time (s)    |
|--------------------------|------------------|------------------------|-------------|------------------|------------------------|-------------|-------------------|-------------------------|-------------|--------------------------|------------------|------------------------|-------------|------------------|------------------------|-------------|------------------|-------------------------|-------------|
| OD-DEAL-200              | <b>30.426691</b> | <b>5.59</b>            | 0.13        | 67.955727        | 1.71                   | <b>0.32</b> | 128.135544        | -0.78                   | 0.66        | OD-DEAL-200              | 11.665637        | 8.78                   | <b>0.06</b> | 18.476112        | 11.26                  | <b>0.16</b> | 28.419750        | 22.06                   | <b>0.40</b> |
| OD-DEAL-noCluster-200    | 30.486713        | 5.79                   | 0.13        | 68.771210        | 2.91                   | 0.48        | 131.132645        | -0.48                   | 1.16        | OD-DEAL-noCluster-200    | <b>11.494427</b> | <b>7.18</b>            | <b>0.06</b> | 18.769777        | 13.03                  | <b>0.16</b> | 30.722218        | 31.95                   | 0.43        |
| OD-DEAL-Transformer-200  | 31.885248        | 10.65                  | 0.14        | 70.307858        | 5.23                   | 0.34        | 131.897873        | -0.10                   | 0.69        | OD-DEAL-Transformer-200  | 11.608491        | 8.24                   | <b>0.06</b> | 18.906697        | 13.85                  | <b>0.16</b> | 31.240973        | 34.18                   | 0.41        |
| OD-DEAL-500              | 31.745686        | 10.16                  | <b>0.13</b> | <b>67.915985</b> | <b>1.65</b>            | <b>0.32</b> | <b>126.895134</b> | <b>-3.70</b>            | <b>0.65</b> | OD-DEAL-500              | 11.728203        | 9.36                   | <b>0.06</b> | 18.708435        | 12.66                  | <b>0.16</b> | 29.465239        | 26.55                   | <b>0.40</b> |
| OD-DEAL-noCluster-500    | 32.247334        | 11.90                  | 0.25        | 68.644653        | 2.74                   | 0.54        | 127.648041        | -3.13                   | 1.16        | OD-DEAL-noCluster-500    | 11.645096        | 8.59                   | <b>0.06</b> | 18.454132        | 11.13                  | 0.17        | 28.058287        | 20.51                   | 0.43        |
| OD-DEAL-Transformer-500  | 32.2414150       | 12.48                  | <b>0.13</b> | 70.100037        | 4.92                   | 0.34        | 130.402588        | -1.04                   | 0.92        | OD-DEAL-Transformer-500  | 11.622268        | 8.37                   | <b>0.06</b> | 18.305189        | 10.23                  | <b>0.16</b> | 28.460236        | 22.24                   | <b>0.40</b> |
| OD-DEAL-1000             | 33.813118        | 17.34                  | <b>0.13</b> | 68.957115        | 3.2                    | <b>0.32</b> | 127.634361        | -3.14                   | 0.66        | OD-DEAL-1000             | 12.740256        | 18.80                  | <b>0.06</b> | 19.815060        | 19.32                  | <b>0.16</b> | 30.033415        | 28.99                   | <b>0.40</b> |
| OD-DEAL-noCluster-1000   | 33.826980        | 16.69                  | 0.25        | 69.569138        | 4.13                   | 0.41        | 129.007950        | -2.10                   | 0.72        | OD-DEAL-noCluster-1000   | 11.639325        | 8.53                   | <b>0.06</b> | <b>18.077166</b> | <b>8.86</b>            | 0.17        | <b>26.993736</b> | <b>15.94</b>            | 0.43        |
| OD-DEAL-Transformer-1000 | 32.548656        | 12.95                  | 0.19        | 70.334396        | 5.27                   | 0.35        | 129.981720        | -1.36                   | 0.67        | OD-DEAL-Transformer-1000 | 11.741479        | 9.48                   | <b>0.06</b> | 18.131119        | 9.18                   | <b>0.16</b> | 27.099134        | 16.39                   | 0.41        |

## D.2. Sensitivity Analysis

 Table 5. Sensitivity analysis of hyperparameter  $\hat{N}$  in OD-DEAL-200 on synthetic CVRP dataset.

| $\hat{N}$ | Obj.      | $ V  = 200$<br>Gap (%) | Time (s) | Obj.      | $ V  = 500$<br>Gap (%) | Time (s) | Obj.       | $ V  = 1000$<br>Gap (%) | Time (s) |
|-----------|-----------|------------------------|----------|-----------|------------------------|----------|------------|-------------------------|----------|
| 10        | 30.592449 | 6.16                   | 0.13     | 68.320488 | 2.26                   | 0.32     | 128.594177 | -2.41                   | 0.64     |
| 30        | 30.519241 | 5.91                   | 0.13     | 68.136040 | 1.98                   | 0.32     | 128.321060 | -2.62                   | 0.64     |
| 50        | 30.509777 | 5.87                   | 0.13     | 68.076363 | 1.89                   | 0.32     | 128.211121 | -2.70                   | 0.63     |
| 70        | 30.457382 | 5.69                   | 0.13     | 68.008392 | 1.79                   | 0.33     | 128.177887 | -2.73                   | 0.66     |
| 100       | 30.426691 | 5.59                   | 0.13     | 67.955727 | 1.71                   | 0.33     | 128.135544 | -2.76                   | 0.66     |
| 110       | 30.424309 | 5.58                   | 0.13     | 67.939011 | 1.69                   | 0.32     | 128.131516 | -2.76                   | 0.66     |
| 130       | 30.429920 | 5.60                   | 0.13     | 67.939133 | 1.69                   | 0.32     | 128.110443 | -2.78                   | 0.66     |
| 150       | 30.423094 | 5.57                   | 0.13     | 67.915329 | 1.65                   | 0.33     | 128.054642 | -2.82                   | 0.65     |
| 170       | 30.421856 | 5.57                   | 0.13     | 67.915901 | 1.65                   | 0.32     | 128.050415 | -2.82                   | 0.66     |
| 200       | 30.399479 | 5.49                   | 0.13     | 67.886208 | 1.61                   | 0.34     | 128.023117 | -2.84                   | 0.65     |
| 210       | 30.376862 | 5.41                   | 0.13     | 67.879105 | 1.60                   | 0.33     | 128.029999 | -2.84                   | 0.65     |
| 230       | 30.379044 | 5.42                   | 0.13     | 67.860344 | 1.57                   | 0.33     | 128.010468 | -2.85                   | 0.66     |
| 250       | 30.360744 | 5.36                   | 0.14     | 67.847359 | 1.55                   | 0.33     | 128.000504 | -2.86                   | 0.66     |
| 270       | 30.346642 | 5.31                   | 0.13     | 67.832977 | 1.53                   | 0.33     | 127.986496 | -2.87                   | 0.66     |
| 300       | 30.342957 | 5.30                   | 0.13     | 67.844048 | 1.54                   | 0.33     | 127.963737 | -2.89                   | 0.66     |
| 310       | 30.342241 | 5.29                   | 0.13     | 67.839523 | 1.54                   | 0.33     | 127.961197 | -2.89                   | 0.66     |
| 330       | 30.339897 | 5.29                   | 0.13     | 67.835999 | 1.53                   | 0.33     | 127.949440 | -2.90                   | 0.66     |
| 350       | 30.336113 | 5.27                   | 0.14     | 67.806686 | 1.49                   | 0.33     | 127.939880 | -2.91                   | 0.66     |
| 370       | 30.329941 | 5.25                   | 0.13     | 67.794609 | 1.47                   | 0.32     | 127.915802 | -2.93                   | 0.66     |
| 400       | 30.326078 | 5.24                   | 0.13     | 67.800224 | 1.48                   | 0.33     | 127.897903 | -2.94                   | 0.67     |
| 410       | 30.314137 | 5.20                   | 0.14     | 67.800354 | 1.48                   | 0.33     | 127.896988 | -2.94                   | 0.67     |
| 430       | 30.337181 | 5.28                   | 0.14     | 67.790215 | 1.46                   | 0.33     | 127.895905 | -2.94                   | 0.67     |
| 450       | 30.336346 | 5.27                   | 0.14     | 67.787231 | 1.46                   | 0.33     | 127.894928 | -2.94                   | 0.67     |
| 470       | 30.317787 | 5.21                   | 0.14     | 67.778030 | 1.44                   | 0.33     | 127.878433 | -2.95                   | 0.67     |
| 500       | 30.315397 | 5.20                   | 0.14     | 67.766273 | 1.43                   | 0.33     | 127.868279 | -2.96                   | 0.67     |
| 510       | 30.302973 | 5.16                   | 0.14     | 67.764465 | 1.42                   | 0.33     | 127.865105 | -2.96                   | 0.67     |
| 530       | 30.322701 | 5.23                   | 0.14     | 67.762535 | 1.42                   | 0.32     | 127.835403 | -2.99                   | 0.68     |
| 550       | 30.320812 | 5.22                   | 0.14     | 67.748512 | 1.40                   | 0.33     | 127.834465 | -2.99                   | 0.68     |
| 570       | 30.315590 | 5.20                   | 0.14     | 67.759621 | 1.42                   | 0.33     | 127.853645 | -2.97                   | 0.69     |
| 600       | 30.308542 | 5.18                   | 0.14     | 67.757469 | 1.41                   | 0.32     | 127.840706 | -2.98                   | 0.69     |
| 610       | 30.307873 | 5.17                   | 0.14     | 67.746513 | 1.40                   | 0.33     | 127.839409 | -2.98                   | 0.69     |
| 630       | 30.307478 | 5.17                   | 0.14     | 67.734108 | 1.38                   | 0.33     | 127.837395 | -2.99                   | 0.71     |
| 650       | 30.303312 | 5.16                   | 0.14     | 67.741791 | 1.39                   | 0.33     | 127.830864 | -2.99                   | 0.71     |
| 670       | 30.310297 | 5.18                   | 0.14     | 67.733635 | 1.38                   | 0.33     | 127.829323 | -2.99                   | 0.71     |
| 700       | 30.310377 | 5.18                   | 0.14     | 67.730736 | 1.37                   | 0.33     | 127.822365 | -3.00                   | 0.72     |
| 800       | 30.303747 | 5.16                   | 0.14     | 67.719322 | 1.36                   | 0.33     | 127.794014 | -3.02                   | 0.75     |
| 900       | 30.289932 | 5.11                   | 0.14     | 67.702599 | 1.33                   | 0.33     | 127.780830 | -3.03                   | 0.78     |
| 1000      | 30.294365 | 5.13                   | 0.14     | 67.689888 | 1.31                   | 0.34     | 127.783363 | -3.03                   | 0.82     |
| 1100      | 30.285315 | 5.10                   | 0.14     | 67.667992 | 1.28                   | 0.34     | 127.761513 | -3.04                   | 0.85     |
| 1200      | 30.280766 | 5.08                   | 0.14     | 67.658775 | 1.27                   | 0.34     | 127.747032 | -3.05                   | 0.89     |
| 1300      | 30.271786 | 5.05                   | 0.14     | 67.653839 | 1.26                   | 0.34     | 127.771690 | -3.04                   | 0.93     |
| 1400      | 30.288689 | 5.11                   | 0.14     | 67.652580 | 1.26                   | 0.37     | 127.754906 | -3.05                   | 1.01     |
| 1500      | 30.284353 | 5.09                   | 0.14     | 67.648216 | 1.25                   | 0.38     | 127.749565 | -3.05                   | 1.04     |
| 1600      | 30.290970 | 5.12                   | 0.14     | 67.659991 | 1.18                   | 0.39     | 127.731415 | -3.07                   | 1.07     |
| 1700      | 30.284948 | 5.09                   | 0.14     | 67.618065 | 1.21                   | 0.39     | 127.725212 | -3.07                   | 1.11     |
| 1800      | 30.282204 | 5.08                   | 0.14     | 67.611877 | 1.20                   | 0.40     | 127.724648 | -3.07                   | 1.14     |

**Sensitivity to  $\hat{N}$ .** Table 5 shows that increasing the number of sampled routes consistently improves solution quality, but with diminishing returns. For example, at  $|V| = 500$ , the optimality gap decreases from 2.26% at  $\hat{N} = 10$  to 1.54% at  $\hat{N} = 300$ , and further to 1.20% at  $\hat{N} = 1800$ , while the runtime increase modestly from 0.32 seconds to 0.40 seconds. A similar trend is observed for  $|V| = 200$  (6.16% to 5.08%) and  $|V| = 1000$  (-2.41% to -3.07%), where the runtime increases from 0.64 seconds to 1.14 seconds. This results indicates that moderate value of  $\hat{N}$  capture most of the performance gains with limited computational overhead.

Table 6. Sensitivity analysis of hyperparameter  $\mathcal{K}$  in OD-DEAL-200 on synthetic CVRP dataset.

| $\mathcal{K}$ | $ V  = 200$ |         |          | $ V  = 500$ |         |          | $ V  = 1000$ |         |          |
|---------------|-------------|---------|----------|-------------|---------|----------|--------------|---------|----------|
|               | Obj.        | Gap (%) | Time (s) | Obj.        | Gap (%) | Time (s) | Obj.         | Gap (%) | Time (s) |
| 20            | 31.350094   | 8.79    | 0.14     | 71.638000   | 7.22    | 0.34     | 141.685013   | 7.52    | 0.68     |
| 30            | 30.533363   | 5.96    | 0.13     | 68.268585   | 2.18    | 0.32     | 132.290024   | 0.39    | 0.67     |
| 40            | 30.426691   | 5.59    | 0.13     | 67.482193   | 1.00    | 0.32     | 128.752258   | -2.29   | 0.65     |
| 50            | 30.450418   | 5.67    | 0.13     | 67.326096   | 0.77    | 0.32     | 127.559982   | -3.20   | 0.65     |
| 60            | 30.564724   | 6.07    | 0.14     | 67.400139   | 0.88    | 0.32     | 127.347626   | -3.36   | 0.65     |

**Sensitivity to  $\mathcal{K}$ .** Table 6 shows that overly sparse neighborhoods hurt performance ( $\mathcal{K} = 20$  yields gaps of 8.79%/7.22%/7.52% for  $|V| = 200/500/1000$ ). Increasing  $\mathcal{K}$  to 40–60 sharply reduces gaps with almost unchanged runtime (about 0.13/0.32/0.65s). The best gaps occur at  $\mathcal{K} = 40$  for  $|V| = 200$  (5.59%),  $\mathcal{K} = 50$  for  $|V| = 500$  (0.77%) and  $\mathcal{K} = 60$  for  $|V| = 1000$  (-3.36%), indicating that a moderate sparsity level is sufficient.

### D.3. Experiments on CVRPLib Benchmarks

We adopted the CVRPLib repository<sup>1</sup> as our evaluation platform. This repository hosts the most authoritative benchmark instances in the CVRP field, covering a wide range of problem scales and diverse topological distributions, serving as a standard testbed for verifying algorithmic robustness and generalization.

**Classic Benchmarks.** We evaluate OD-DEAL on standard benchmark instances from CVRPLib (Sets A, B, E, P, and tai), which are widely used in the literature (Augerat et al., 1995; Christofides, 1979; Rochat & Taillard, 1995). Detailed results are summarized in Tables 7 through 10. We choose these five sets because most instances provide known optimal solutions. The uniform EUC\_2D format ensures consistent preprocessing and evaluation protocols. These sets represent standard CVRP configurations without extra constraints. The problem scope aligns with the operational requirements of both OD-DEAL and the evaluated baselines. OD-DEAL demonstrates strong generalization across all benchmark sets, consistently achieving substantially smaller optimality gaps than AGFN. For instance, on Set B, the average gap is dramatically reduced from 195.72% (AGFN) to 29.46% (OD-DEAL), and on Set P, the gap decreases from 81.77% to 19.60%. Furthermore, OD-DEAL consistently maintains sub-second inference latency (ranging from approximately 0.43s to 0.50s), outperforming GLOP (ranging from approximately 0.72s to 0.76s) in efficiency, thereby verifying the algorithm’s adaptability and speed under varying data characteristics.

**XL instances<sup>2</sup> (Queiroga et al., 2026).** We also introduce the newly released XL dataset. Table 12 evaluates OD-DEAL-200 on 100 XL instances (1000 to 10000 nodes) with ten runs per instance. OD-DEAL yields smaller gaps than AGFN on 63/100 instances and avoids AGFN’s extreme failures (e.g., 238.40% at XL-n1981-k13 and 408.96% at XL-n6034-k61), while remaining faster than GFACS on every instance (e.g., 11.30s vs 43.30s at XL-n10001-k1570). GFACS achieves the smallest gaps on most instances (97/100) but at higher runtime, whereas OD-DEAL maintains a better quality-efficiency balance and shows low variance across runs (best and mean are nearly identical).

<sup>1</sup><https://galgos.inf.puc-rio.br/cvrplib/index.php/en/instances>

<sup>2</sup>The XL instances for CXVRP are obtained from CVRPLIB, which released a benchmark set in 2026 comprising 100 challenging CVRP instances ranging from 1000 to 10000 customers.

*Table 7.* Results on A instances: 10 independent runs per instance.

| Instance  | Optimal |      |         |         | OD-DEAL-200 |         |         |         | AGFN-200 |         |         |         | GFACS-200 |         |         |         | GL-OP |      |     |      |
|-----------|---------|------|---------|---------|-------------|---------|---------|---------|----------|---------|---------|---------|-----------|---------|---------|---------|-------|------|-----|------|
|           | Obj     | Best | Mean    | Gap     | Best        | Mean    | Gap     | Time    | Best     | Mean    | Gap     | Time    | Best      | Mean    | Gap     | Time    | Best  | Mean | Gap | Time |
| A-n32-k5  | 784.00  | -    | 852.00  | 886.20  | 8.67        | 0.43    | 3174.00 | 3352.20 | 304.85   | 0.44    | 785.00  | 785.00  | 0.13      | 93      | 1129.00 | 1225.90 | 44.01 | 0.71 |     |      |
| A-n33-k5  | 661.00  | -    | 866.00  | 880.20  | 31.01       | 0.43    | 765.00  | 787.30  | 15.73    | 0.42    | 661.30  | 661.30  | 0.00      | 98      | 1012.00 | 1116.90 | 53.10 | 0.71 |     |      |
| A-n33-k6  | 742.00  | -    | 1008.00 | 1034.10 | 35.05       | 0.43    | 861.00  | 862.80  | 1.04     | 0.41    | 742.00  | 742.00  | 0.00      | 1.03    | 1067.00 | 1166.40 | 43.80 | 0.71 |     |      |
| A-n34-k5  | 778.00  | -    | 927.00  | 986.80  | 19.15       | 0.43    | 914.00  | 981.30  | 17.48    | 0.42    | 779.00  | 779.00  | 0.13      | 102     | 1130.00 | 1184.70 | 45.24 | 0.71 |     |      |
| A-n34-k6  | 779.00  | -    | 1059.00 | 1272.00 | 32.54       | 0.43    | 755.00  | 3325.00 | 297.37   | 0.44    | 769.00  | 799.00  | 0.00      | 1.04    | 1076.00 | 1231.80 | 47.18 | 0.71 |     |      |
| A-n34-k7  | 669.00  | -    | 920.00  | 1005.80 | 37.52       | 0.43    | 744.00  | 785.30  | 121.21   | 0.42    | 670.00  | 670.00  | 0.15      | 1.08    | 1046.00 | 1114.50 | 56.35 | 0.71 |     |      |
| A-n35-k6  | 949.00  | -    | 1184.00 | 1293.40 | 24.76       | 0.43    | 1094.00 | 1270.50 | 15.28    | 0.42    | 949.00  | 950.80  | 0.00      | 1.10    | 1313.00 | 1418.40 | 38.36 | 0.71 |     |      |
| A-n35-k7  | 730.00  | -    | 929.00  | 943.00  | 24.76       | 0.43    | 901.00  | 1002.40 | 12.42    | 0.42    | 730.00  | 730.00  | 0.00      | 1.10    | 1119.00 | 1210.50 | 59.72 | 0.71 |     |      |
| A-n36-k5  | 822.00  | -    | 1040.00 | 1089.80 | 26.52       | 0.44    | 998.00  | 1051.90 | 21.41    | 0.41    | 822.00  | 823.80  | 0.00      | 1.13    | 1235.00 | 1313.60 | 50.24 | 0.71 |     |      |
| A-n36-k6  | 831.00  | -    | 952.00  | 1003.00 | 14.56       | 0.43    | 968.00  | 1102.40 | 16.49    | 0.42    | 835.00  | 835.00  | 0.48      | 1.10    | 1286.00 | 1369.30 | 54.75 | 0.71 |     |      |
| A-n36-k7  | 937.00  | -    | 1112.00 | 1155.30 | 18.68       | 0.43    | 1095.00 | 1132.30 | 15.00    | 0.42    | 937.00  | 938.00  | 0.00      | 1.17    | 1517.00 | 1548.80 | 61.90 | 0.71 |     |      |
| A-n45-k6  | 944.00  | -    | 1021.00 | 1041.10 | 8.16        | 0.44    | 1122.00 | 1195.00 | 18.86    | 0.42    | 953.00  | 954.90  | 0.99      | 1.22    | 1552.00 | 1641.50 | 64.83 | 0.71 |     |      |
| A-n45-k7  | 1146.00 | -    | 1237.00 | 1330.60 | 7.94        | 0.44    | 2604.00 | 2845.60 | 127.23   | 0.44    | 1147.00 | 1152.50 | 0.09      | 1.21    | 1623.00 | 1709.20 | 41.62 | 0.71 |     |      |
| A-n46-k6  | 914.00  | -    | 997.00  | 1056.80 | 9.08        | 0.44    | 1026.00 | 1044.00 | 12.53    | 0.45    | 914.00  | 916.70  | 0.00      | 1.26    | 1390.00 | 1353.50 | 52.08 | 0.72 |     |      |
| A-n46-k7  | 1073.00 | -    | 1286.00 | 1384.80 | 19.85       | 0.44    | 1502.00 | 1644.60 | 39.98    | 0.43    | 1073.00 | 1079.10 | 0.00      | 1.26    | 1656.00 | 1750.60 | 54.33 | 0.72 |     |      |
| A-n53-k7  | 10.00   | -    | 1116.00 | 1147.90 | 10.50       | 0.43    | 1335.00 | 1396.10 | 32.18    | 0.43    | 1071.00 | 1071.00 | 0.69      | 1.34    | 1642.00 | 1759.40 | 62.57 | 0.72 |     |      |
| A-n54-k7  | 116.00  | -    | 1293.00 | 1298.30 | 10.80       | 0.43    | 1492.00 | 1667.50 | 27.85    | 0.44    | 1167.00 | 1175.00 | 0.00      | 1.35    | 1793.00 | 1862.00 | 53.64 | 0.72 |     |      |
| A-n55-k9  | 1073.00 | -    | 1248.00 | 1276.30 | 16.31       | 0.44    | 1213.00 | 1247.80 | 13.05    | 0.44    | 1073.00 | 1073.90 | 0.00      | 1.42    | 1823.00 | 1981.20 | 69.90 | 0.72 |     |      |
| A-n60-k9  | 1354.00 | -    | 1427.00 | 1451.00 | 5.79        | 0.44    | 1555.00 | 1585.80 | 13.37    | 0.44    | 1358.00 | 1359.30 | 0.00      | 1.47    | 2108.00 | 2205.60 | 55.69 | 0.72 |     |      |
| A-n62-k8  | 1034.00 | -    | 1112.00 | 1162.50 | 0.44        | 1195.00 | 1227.00 | 15.57   | 0.44     | 1035.00 | 1042.10 | 0.10    | 1.53      | 1758.00 | 1854.70 | 70.02   | 0.72  |      |     |      |
| A-n62-k8  | 1288.00 | -    | 1386.00 | 1417.10 | 7.61        | 0.44    | 1568.00 | 1605.80 | 21.74    | 0.44    | 1304.00 | 1307.70 | 0.24      | 1.43    | 2096.00 | 2222.60 | 62.73 | 0.73 |     |      |
| A-n63-k9  | 1314.00 | -    | 1424.00 | 1475.80 | 8.70        | 0.44    | 1461.00 | 1525.80 | 11.19    | 0.44    | 1318.00 | 1320.80 | 0.38      | 1.24    | 2024.00 | 2225.60 | 61.64 | 0.72 |     |      |
| A-n64-k9  | 1616.00 | -    | 1742.00 | 1787.80 | 7.80        | 0.44    | 1709.00 | 1551.65 | 20.65    | 0.44    | 1621.00 | 1630.40 | 0.31      | 1.54    | 2039.00 | 2449.50 | 47.09 | 0.72 |     |      |
| A-n64-k9  | 1401.00 | -    | 1590.00 | 1627.00 | 13.49       | 0.44    | 1620.00 | 1691.70 | 1.56     | 0.44    | 1411.00 | 1423.10 | 0.71      | 1.59    | 2104.00 | 2207.50 | 50.18 | 0.72 |     |      |
| A-n65-k9  | 1174.00 | -    | 1368.00 | 1465.70 | 16.52       | 0.44    | 1319.00 | 1375.20 | 15.35    | 0.44    | 1178.00 | 1179.60 | 0.34      | 1.52    | 1161.00 | 1804.20 | 70.24 | 0.73 |     |      |
| A-n80-k10 | 1763.00 | -    | 1304.00 | 1813.30 | 12.51       | 0.44    | 129.00  | 1318.00 | 11.39    | 0.45    | 1163.00 | 1167.30 | 0.35      | 1.65    | 2121.00 | 2199.80 | 83.00 | 0.73 |     |      |
| Average   | 1041.93 | -    | 1197.44 | 1250.62 | 16.59       | 0.44    | 1549.11 | 1649.62 | 49.74    | 0.43    | 1045.00 | 1047.80 | 0.26      | 1.29    | 1633.59 | 1779.00 | 56.15 | 0.72 |     |      |

**Table 8** Results on E instances: 10 independent runs per instance

| Instance     | Optimal |        |         | OD-DEAL-200 |       |         | AGFN-200 |         |        | GFACS-200 |         |         | GLOP |         |         |         |       |      |
|--------------|---------|--------|---------|-------------|-------|---------|----------|---------|--------|-----------|---------|---------|------|---------|---------|---------|-------|------|
|              | Obj     | Gap    | Best    | Mean        | Gap   | Time    | Best     | Mean    | Gap    | Best      | Mean    | Gap     | Best | Mean    | Gap     |         |       |      |
| E-n101-k14   | 106700  | -      | 1215.00 | 1247.40     | 13.87 | 0.47    | 1289.00  | 1317.50 | 20.81  | 0.47      | 1088.00 | 1096.00 | 1.97 | 2.30    | 2096.00 | 2161.20 | 96.44 | 0.74 |
| E-E-n101-k18 | 815.00  | -      | 950.00  | 962.30      | 16.56 | 0.46    | 1052.00  | 1073.90 | 29.08  | 0.47      | 818.00  | 821.10  | 0.37 | 1.99    | 1614.00 | 1634.40 | 98.04 | 0.74 |
| E-E-n102-k4  | 375.00  | -      | 452.00  | 207.20      | 50.53 | 0.41    | 450.00   | 457.00  | 16.27  | 0.40      | 375.00  | 375.00  | 0.00 | 52.00   | 565.70  | 583.90  | 0.71  | 0.71 |
| E-E-n23-k3   | 569.00  | -      | 901.00  | 977.00      | 58.35 | 0.41    | 1414.00  | 1580.40 | 148.51 | 0.42      | 569.90  | 569.90  | 0.00 | 675.00  | 769.80  | 18.63   | 0.71  | 0.71 |
| E-E-n33-k4   | 835.00  | -      | 1349.00 | 1570.60     | 61.56 | 0.43    | 4768.00  | 4952.90 | 471.02 | 0.43      | 835.10  | 835.10  | 0.00 | 987.00  | 1063.00 | 18.20   | 0.71  | 0.71 |
| E-E-n51-k5   | 521.00  | -      | 680.00  | 887.00      | 30.52 | 0.44    | 617.00   | 655.90  | 13.73  | 0.43      | 521.00  | 521.00  | 0.00 | 1.24    | 510.70  | 59.50   | 34.72 | 0.71 |
| E-E-n76-k10  | 830.00  | -      | 931.00  | 965.00      | 1.17  | 0.44    | 941.00   | 974.00  | 13.73  | 0.45      | 839.00  | 845.80  | 1.08 | 1.80    | 1530.00 | 1590.80 | 84.34 | 0.73 |
| E-E-n76-k14  | 1021.00 | -      | 1086.00 | 1094.40     | 6.37  | 0.45    | 1176.00  | 1267.30 | 15.18  | 0.45      | 1034.00 | 1037.80 | 1.27 | 1.97    | 1714.00 | 1844.70 | 67.78 | 0.73 |
| E-E-n76-k18  | 735.00  | -      | 785.00  | 806.00      | 15.10 | 0.45    | 806.00   | 813.00  | 20.54  | 0.45      | 622.00  | 622.00  | 0.00 | 1.61    | 678.00  | 873.90  | 0.72  | 0.72 |
| Average      |         | 922.30 | 977.39  | 25.39       | 0.44  | 1341.30 | 1405.52  | 77.54   | 0.44   | 750.10    | 753.24  | 0.54    | 1.50 | 1260.90 | 1337.66 | 65.48   | 0.72  |      |

Table 9. Results on B instances: 10 independent runs per instance.

| Instance  | Optimal |     |          | OD-DEAL-200 |       |         | AGFN-200 |         |         | GFACS-200 |         |         | GLOP    |         |         |         |         |       |      |
|-----------|---------|-----|----------|-------------|-------|---------|----------|---------|---------|-----------|---------|---------|---------|---------|---------|---------|---------|-------|------|
|           | Obj     | Gap | Best     | Mean        | Gap   | Time    | Best     | Mean    | Gap     | Time      | Best    | Mean    | Gap     | Time    |         |         |         |       |      |
| B-n31-k5  | 672.00  | -   | 752.00   | 11.90       | 0.43  | 3229.00 | 3385.00  | 380.51  | 0.43    | 672.00    | 673.70  | 0.00    | 0.87    | 931.00  | 986.30  | 38.54   | 0.71    |       |      |
| B-n34-k5  | 788.00  | -   | 908.00   | 1045.20     | 15.23 | 0.43    | 3581.00  | 3848.50 | 354.44  | 0.44      | 788.00  | 788.00  | 0.00    | 0.91    | 1002.00 | 1100.40 | 27.16   | 0.71  |      |
| B-n35-k5  | 955.00  | -   | 1103.00  | 1192.30     | 15.50 | 0.43    | 4415.00  | 4753.10 | 362.30  | 0.44      | 955.30  | 0.00    | 0.94    | 1208.00 | 1383.90 | 26.49   | 0.71    |       |      |
| B-n38-k6  | 805.00  | -   | 875.00   | 1012.00     | 8.70  | 0.43    | 873.00   | 882.50  | 8.45    | 0.42      | 806.00  | 806.00  | 0.00    | 1.04    | 1137.00 | 1240.20 | 41.24   | 0.71  |      |
| B-n39-k5  | 549.00  | -   | 693.00   | 720.50      | 26.23 | 0.43    | 870.00   | 987.40  | 58.47   | 0.42      | 550.00  | 550.00  | 0.18    | 1.02    | 941.00  | 1073.40 | 71.40   | 0.71  |      |
| B-n41-k6  | 829.00  | -   | 921.00   | 983.90      | 11.10 | 0.44    | 1365.00  | 1542.90 | 64.66   | 0.43      | 831.00  | 834.30  | 0.24    | 1.08    | 1349.00 | 1419.80 | 62.73   | 0.71  |      |
| B-n43-k6  | 742.00  | -   | 828.00   | 923.30      | 11.59 | 0.43    | 907.00   | 972.70  | 22.24   | 0.42      | 742.00  | 744.70  | 0.00    | 1.14    | 1033.00 | 1142.00 | 39.22   | 0.72  |      |
| B-n44-k7  | 909.00  | -   | 1076.00  | 1142.70     | 18.37 | 0.44    | 2008.00  | 2293.00 | 120.90  | 0.43      | 910.00  | 910.00  | 0.00    | 1.17    | 1366.00 | 1473.00 | 50.28   | 0.71  |      |
| B-n45-k5  | 751.00  | -   | 859.00   | 971.40      | 14.38 | 0.44    | 917.00   | 932.50  | 22.10   | 0.43      | 751.00  | 751.00  | 0.00    | 1.15    | 1190.00 | 1303.40 | 58.46   | 0.71  |      |
| B-n45-k6  | 678.00  | -   | 825.00   | 949.00      | 21.68 | 0.44    | 824.00   | 854.10  | 21.53   | 0.42      | 681.00  | 710.30  | 0.44    | 1.19    | 1040.00 | 1138.70 | 53.39   | 0.71  |      |
| B-n50-k7  | 741.00  | -   | 865.00   | 879.80      | 16.73 | 0.43    | 865.00   | 920.40  | 16.73   | 0.43      | 741.00  | 741.00  | 0.00    | 1.25    | 1379.00 | 1487.80 | 86.10   | 0.72  |      |
| B-n50-k8  | 1312.00 | -   | 1496.00  | 1546.50     | 14.02 | 0.44    | 1404.00  | 1422.30 | 7.01    | 0.43      | 1319.00 | 1322.50 | 0.53    | 1.33    | 1778.00 | 1874.90 | 35.52   | 0.72  |      |
| B-n52-k7  | 747.00  | -   | 829.00   | 922.70      | 10.98 | 0.44    | 827.00   | 835.90  | 10.71   | 0.43      | 748.60  | 748.60  | 0.13    | 1.27    | 1326.00 | 1497.70 | 77.51   | 0.72  |      |
| B-n56-k7  | 707.00  | -   | 839.00   | 863.50      | 18.67 | 0.44    | 812.00   | 827.30  | 14.85   | 0.44      | 709.90  | 711.00  | 0.28    | 1.38    | 1556.00 | 1470.50 | 91.80   | 0.72  |      |
| B-n57-k9  | 1598.00 | -   | 1814.00  | 1983.60     | 13.52 | 0.44    | 1690.40  | 1769.50 | 7894.50 | 0.44      | 1601.00 | 1602.80 | 0.19    | 1.38    | 2208.00 | 2305.40 | 38.17   | 0.72  |      |
| B-n63-k10 | 1496.00 | -   | 1621.00  | 1692.00     | 8.36  | 0.44    | 174.00   | 3796.00 | 4038.10 | 153.74    | 0.45    | 1557.00 | 1540.20 | 2.74    | 1.58    | 2385.00 | 2468.40 | 59.43 | 0.72 |
| B-n64-k9  | 861.00  | -   | 977.00   | 1018.90     | 13.47 | 0.44    | 1148.00  | 1181.90 | 33.33   | 0.45      | 877.90  | 883.40  | 2.09    | 1.58    | 1696.00 | 1795.90 | 96.98   | 0.72  |      |
| B-n66-k9  | 1316.00 | -   | 1565.00  | 1613.80     | 18.92 | 0.45    | 1521.00  | 1523.70 | 65.27   | 0.45      | 1321.00 | 1323.70 | 0.38    | 1.59    | 2023.00 | 2108.00 | 53.72   | 0.72  |      |
| B-n67-k10 | 1032.00 | -   | 1193.00  | 1284.90     | 15.60 | 0.44    | 1653.00  | 1720.80 | 60.17   | 0.46      | 1036.00 | 1043.90 | 0.39    | 1.63    | 1912.00 | 2049.10 | 85.27   | 0.73  |      |
| B-n68-k9  | 1272.00 | -   | 1408.00  | 1546.10     | 10.69 | 0.44    | 1539.00  | 1644.50 | 20.99   | 0.45      | 1289.00 | 1293.40 | 1.34    | 1.51    | 2065.00 | 2149.60 | 62.34   | 0.72  |      |
| B-n78-k10 | 1221.00 | -   | 1370.00  | 1436.60     | 12.20 | 0.45    | 1368.00  | 1483.00 | 12.04   | 0.45      | 1223.00 | 1231.60 | 0.16    | 1.77    | 2299.00 | 2388.50 | 88.29   | 0.73  |      |
| Average   | 951.48  | -   | 11086.52 | 1165.77     | 14.66 | 0.44    | 2012.67  | 2137.81 | 104.37  | 0.44      | 956.62  | 960.26  | 0.44    | 1.28    | 1505.90 | 1612.23 | 59.24   | 0.72  |      |

Table 10. Results on tai instances: 10 independent runs per instance.

| Instance | Optimal  |     |          | OD-DEAL-200 |       |      | AGFN-200 |          |       | GFACS-200 |          |          | GLOP |         |          |          |        |      |
|----------|----------|-----|----------|-------------|-------|------|----------|----------|-------|-----------|----------|----------|------|---------|----------|----------|--------|------|
|          | Obj      | Gap | Best     | Mean        | Gap   | Time | Best     | Mean     | Gap   | Time      | Best     | Mean     | Gap  | Time    |          |          |        |      |
| tai100a  | 2041.34  | -   | 2291.00  | 2332.10     | 12.23 | 0.47 | 2541.00  | 2777.40  | 24.48 | 0.47      | 2076.30  | 1.40     | 2.25 | 3938.00 | 4065.70  | 92.91    | 0.75   |      |
| tai100b  | 1939.90  | -   | 2279.00  | 2321.30     | 17.48 | 0.47 | 2827.00  | 2870.60  | 45.73 | 0.48      | 1940.00  | 1944.70  | 0.01 | 2.18    | 3661.00  | 3887.00  | 88.72  | 0.74 |
| tai100c  | 1406.20  | -   | 2131.00  | 2190.20     | 51.54 | 0.48 | 1889.00  | 1914.90  | 34.33 | 0.48      | 1411.00  | 1416.80  | 0.34 | 2.12    | 3174.00  | 3423.20  | 125.71 | 0.74 |
| tai100d  | 1580.46  | -   | 1837.00  | 1873.00     | 16.23 | 0.47 | 2639.00  | 2698.20  | 66.98 | 0.48      | 1592.00  | 1599.90  | 0.73 | 2.16    | 2995.00  | 3165.80  | 89.50  | 0.75 |
| tai100e  | 3055.23  | -   | 3552.00  | 3585.50     | 15.61 | 0.50 | 3991.00  | 4236.70  | 30.63 | 0.50      | 3135.00  | 3174.70  | 2.61 | 3.13    | 6600.00  | 6802.30  | 116.02 | 0.76 |
| tai100f  | 2727.03  | -   | 3104.00  | 3183.70     | 13.82 | 0.50 | 4535.00  | 4702.80  | 66.30 | 0.51      | 2747.00  | 2765.80  | 0.73 | 3.02    | 5954.00  | 6577.70  | 118.33 | 0.76 |
| tai100g  | 2358.66  | -   | 3051.00  | 3142.60     | 29.35 | 0.50 | 3603.00  | 3680.50  | 52.76 | 0.52      | 2389.00  | 2408.10  | 1.29 | 3.00    | 6229.00  | 6490.10  | 164.09 | 0.77 |
| tai100h  | 2645.39  | -   | 3104.00  | 3154.70     | 17.34 | 0.50 | 4228.00  | 4291.20  | 59.83 | 0.52      | 2695.00  | 2715.90  | 1.88 | 2.90    | 5813.00  | 6157.30  | 119.74 | 0.77 |
| tai385   | 24366.41 | -   | 28244.00 | 28464.40    | 15.91 | 0.66 | 3683.00  | 37153.30 | 51.15 | 0.68      | 25167.00 | 25278.80 | 3.29 | 7.39    | 59418.00 | 61313.30 | 143.85 | 0.88 |
| tai75c   | 1291.01  | -   | 1556.00  | 1658.90     | 20.53 | 0.45 | 1907.00  | 2033.30  | 47.71 | 0.46      | 1292.00  | 1300.20  | 0.08 | 1.73    | 2431.00  | 2520.20  | 88.30  | 0.73 |
| Average  | 4341.16  | -   | 5112.90  | 5190.64     | 21.00 | 0.50 | 6499.10  | 6635.89  | 47.99 | 0.51      | 4443.80  | 4468.12  | 1.24 | 2.99    | 10021.30 | 10440.26 | 114.72 | 0.76 |

Table 11. Results on P instances: 10 independent runs per instance.

| Instance  | Optimal Obj | Gap | OD-DEAL-200 |         |       | AGFN-200 |         |         | GFACS-200 |      |        | GLOP   |       |      |
|-----------|-------------|-----|-------------|---------|-------|----------|---------|---------|-----------|------|--------|--------|-------|------|
|           |             |     | Best        | Mean    | Gap   | Time     | Best    | Mean    | Gap       | Time | Best   | Mean   | Gap   | Time |
| P-n101-k4 | 681.00      | -   | 821.00      | 861.70  | 20.56 | 0.46     | 893.00  | 922.40  | 311.13    | 0.47 | 681.00 | 683.30 | 0.00  | 1.89 |
| P-n16-k8  | 450.00      | -   | 481.00      | 492.80  | 6.89  | 0.41     | 645.00  | 723.80  | 43.33     | 0.41 | 450.00 | 450.00 | 0.00  | 0.80 |
| P-n19-k2  | 212.00      | -   | 315.00      | 350.50  | 48.58 | 0.41     | 809.00  | 912.30  | 281.60    | 0.41 | 212.00 | 212.00 | 0.00  | 0.62 |
| P-n20-k2  | 216.00      | -   | 391.00      | 468.20  | 81.02 | 0.41     | 891.00  | 980.70  | 312.50    | 0.42 | 216.00 | 216.00 | 0.00  | 0.63 |
| P-n21-k2  | 211.00      | -   | 249.00      | 266.10  | 18.01 | 0.40     | 924.00  | 1008.00 | 337.91    | 0.42 | 211.00 | 211.00 | 0.00  | 0.67 |
| P-n22-k2  | 216.00      | -   | 302.00      | 342.90  | 39.81 | 0.40     | 949.00  | 1042.90 | 339.35    | 0.42 | 216.00 | 216.00 | 0.00  | 0.69 |
| P-n23-k8  | 529.00      | -   | 546.00      | 550.20  | 3.21  | 0.41     | 984.00  | 1053.40 | 86.01     | 0.42 | 529.00 | 531.50 | 0.00  | 0.90 |
| P-n40-k5  | 458.00      | -   | 520.00      | 520.00  | 13.54 | 0.43     | 564.00  | 600.90  | 23.14     | 0.42 | 458.00 | 458.00 | 0.00  | 1.06 |
| P-n45-k5  | 510.00      | -   | 605.00      | 622.00  | 18.63 | 0.44     | 578.00  | 600.60  | 13.33     | 0.43 | 510.00 | 510.00 | 0.00  | 1.13 |
| P-n50-k10 | 696.00      | -   | 761.00      | 781.00  | 9.34  | 0.45     | 833.00  | 879.60  | 19.68     | 0.44 | 697.00 | 701.90 | 0.14  | 1.47 |
| P-n50-k7  | 554.00      | -   | 612.00      | 631.80  | 10.47 | 0.44     | 639.00  | 668.40  | 15.34     | 0.43 | 555.00 | 555.80 | 0.18  | 1.27 |
| P-n51-k10 | 741.00      | -   | 773.00      | 796.40  | 4.32  | 0.44     | 801.00  | 814.70  | 8.10      | 0.43 | 744.00 | 746.80 | 0.40  | 1.40 |
| P-n55-k10 | 694.00      | -   | 771.00      | 793.30  | 11.10 | 0.43     | 759.00  | 818.50  | 9.37      | 0.43 | 698.00 | 700.30 | 0.58  | 1.49 |
| P-n55-k7  | 568.00      | -   | 715.00      | 741.70  | 25.88 | 0.43     | 637.00  | 666.90  | 12.15     | 0.43 | 571.00 | 574.90 | 0.53  | 1.34 |
| P-n60-k10 | 744.00      | -   | 812.00      | 843.40  | 9.14  | 0.44     | 836.00  | 903.80  | 15.05     | 0.44 | 744.00 | 752.90 | 0.00  | 1.54 |
| P-n60-k15 | 968.00      | -   | 1055.00     | 1092.50 | 8.99  | 0.44     | 1108.00 | 1136.00 | 14.46     | 0.45 | 973.00 | 976.40 | 0.52  | 1.64 |
| P-n65-k10 | 792.00      | -   | 873.00      | 908.30  | 10.23 | 0.44     | 914.00  | 946.80  | 15.40     | 0.44 | 796.00 | 800.60 | 0.51  | 1.60 |
| P-n70-k10 | 827.00      | -   | 909.00      | 946.50  | 9.92  | 0.45     | 935.00  | 949.80  | 13.06     | 0.45 | 832.00 | 842.30 | 0.60  | 1.70 |
| P-n76-k4  | 593.00      | -   | 705.00      | 721.80  | 18.89 | 0.45     | 721.00  | 788.10  | 21.59     | 0.45 | 595.00 | 599.10 | 0.34  | 1.55 |
| P-n76-k5  | 627.00      | -   | 774.00      | 803.80  | 23.44 | 0.45     | 770.00  | 813.60  | 22.81     | 0.45 | 630.00 | 633.90 | 0.48  | 1.59 |
| Average   | 564.35      | -   | 649.50      | 676.74  | 19.60 | 0.43     | 810.50  | 861.56  | 81.77     | 0.43 | 565.90 | 568.63 | 0.21  | 1.25 |
|           |             |     |             |         |       |          |         |         |           |      | 896.10 | 948.25 | 51.79 | 0.72 |

Table 12. Results on XL instances: 10 independent runs per instance (Part I).

| Instance       | Optimal |           |     | OD-DEAL-200 |             |       | AGFN-200 |             |             |        |      |
|----------------|---------|-----------|-----|-------------|-------------|-------|----------|-------------|-------------|--------|------|
|                | Best    | Mean      | Gap | Best        | Mean        | Gap   | Time     | Best        | Mean        | Gap    | Time |
| XL-n1048-k237  | 380211  | 380369.4  | -   | 410043.654  | 410043.654  | 7.80  | 1.24     | 586600.288  | 589136.749  | 54.89  | 1.25 |
| XL-n1094-k157  | 112431  | 112452.6  | -   | 121001.248  | 121001.248  | 7.60  | 1.23     | 134172.017  | 134172.017  | 19.31  | 1.22 |
| XL-n1141-k112  | 95727   | 95798.9   | -   | 109660.142  | 109660.142  | 14.47 | 1.24     | 114116.610  | 114116.610  | 19.12  | 1.19 |
| XL-n1188-k96   | 104415  | 104511.6  | -   | 120532.764  | 120560.140  | 15.36 | 1.26     | 118267.754  | 118267.754  | 13.16  | 1.18 |
| XL-n1234-k55   | 96647   | 96787.3   | -   | 118613.753  | 118613.753  | 22.55 | 1.25     | 109826.823  | 109826.823  | 13.47  | 1.18 |
| XL-n1281-k29   | 31101   | 31174.1   | -   | 41950.915   | 41950.915   | 34.57 | 1.27     | 72361.631   | 72415.798   | 132.29 | 1.27 |
| XL-n1328-k19   | 38247   | 38315.0   | -   | 54831.861   | 54831.861   | 43.11 | 1.28     | 55897.893   | 55897.893   | 45.89  | 1.21 |
| XL-n1374-k278  | 233049  | 233248.0  | -   | 258653.259  | 258653.259  | 10.89 | 1.49     | 267887.660  | 267887.660  | 14.85  | 1.41 |
| XL-n1421-k232  | 384826  | 384949.2  | -   | 403384.119  | 403384.119  | 4.79  | 1.48     | 413798.305  | 414620.311  | 7.71   | 1.42 |
| XL-n1468-k151  | 250166  | 250305.2  | -   | 273495.608  | 273495.608  | 9.26  | 1.46     | 266722.418  | 266722.418  | 6.56   | 1.38 |
| XL-n1514-k106  | 92425   | 92489.7   | -   | 107782.714  | 107782.714  | 16.53 | 1.48     | 122313.666  | 122313.666  | 32.25  | 1.44 |
| XL-n1561-k75   | 101549  | 101583.3  | -   | 111553.451  | 111553.451  | 9.81  | 1.47     | 115136.505  | 115853.339  | 14.05  | 1.39 |
| XL-n1608-k39   | 48021   | 48064.3   | -   | 65818.319   | 65818.319   | 36.94 | 1.49     | 86933.603   | 86933.603   | 80.87  | 1.47 |
| XL-n1654-k11   | 36385   | 36429.1   | -   | 58863.340   | 58863.340   | 61.58 | 1.50     | 59098.450   | 59098.450   | 62.23  | 1.41 |
| XL-n1701-k562  | 521136  | 521380.5  | -   | 579554.822  | 579554.822  | 11.16 | 1.94     | 578627.264  | 578627.264  | 10.98  | 1.86 |
| XL-n1748-k271  | 173896  | 174027.2  | -   | 190972.667  | 191059.704  | 9.79  | 1.74     | 208310.833  | 208380.606  | 19.74  | 1.69 |
| XL-n1794-k163  | 141729  | 141777.6  | -   | 162016.203  | 162016.203  | 14.27 | 1.70     | 161006.117  | 161006.117  | 13.56  | 1.65 |
| XL-n1841-k126  | 214038  | 214142.6  | -   | 235810.618  | 235810.618  | 10.12 | 1.73     | 240432.599  | 240432.599  | 12.28  | 1.63 |
| XL-n1888-k82   | 143623  | 143733.5  | -   | 167552.543  | 167552.543  | 16.57 | 1.72     | 160939.960  | 160939.960  | 11.97  | 1.63 |
| XL-n1934-k46   | 53013   | 53067.3   | -   | 68066.924   | 68315.505   | 28.73 | 1.75     | 75222.681   | 75222.681   | 41.75  | 1.67 |
| XL-n1981-k13   | 32580   | 32639.1   | -   | 47033.936   | 47033.936   | 44.10 | 1.77     | 110449.829  | 110449.829  | 238.40 | 1.81 |
| XL-n2028-k617  | 544403  | 544596.6  | -   | 593412.715  | 593517.665  | 8.98  | 2.23     | 588308.310  | 588308.310  | 8.03   | 2.13 |
| XL-n2074-k264  | 421627  | 421805.0  | -   | 446420.070  | 446420.070  | 5.84  | 2.04     | 449275.986  | 449275.986  | 6.51   | 1.94 |
| XL-n2121-k186  | 283211  | 283323.6  | -   | 304575.333  | 304575.333  | 7.50  | 2.00     | 302712.795  | 302712.795  | 6.84   | 1.91 |
| XL-n2168-k138  | 127298  | 127450.2  | -   | 159289.442  | 159289.442  | 24.98 | 2.03     | 156892.847  | 156892.847  | 23.10  | 1.95 |
| XL-n2214-k131  | 154676  | 154722.4  | -   | 169180.937  | 169180.937  | 9.34  | 2.06     | 169082.221  | 169082.221  | 9.28   | 1.95 |
| XL-n2261-k54   | 98907   | 98993.6   | -   | 119713.024  | 119713.024  | 20.93 | 2.03     | 120284.302  | 120284.302  | 21.51  | 1.93 |
| XL-n2307-k34   | 47958   | 48020.2   | -   | 74513.829   | 74513.829   | 55.17 | 2.07     | 86594.827   | 86594.827   | 80.33  | 2.04 |
| XL-n2354-k631  | 940825  | 940960.9  | -   | 1012380.358 | 1012398.856 | 7.59  | 2.56     | 1002710.335 | 1002710.335 | 6.56   | 2.47 |
| XL-n2401-k408  | 463473  | 463673.4  | -   | 493992.770  | 493992.770  | 6.54  | 2.42     | 504150.670  | 504150.670  | 8.73   | 2.33 |
| XL-n2447-k290  | 218706  | 218821.4  | -   | 250624.988  | 250624.988  | 14.53 | 2.41     | 279165.961  | 279165.961  | 27.58  | 2.35 |
| XL-n2494-k194  | 361205  | 361273.1  | -   | 377420.913  | 377420.913  | 4.47  | 2.34     | 381355.143  | 381355.143  | 5.56   | 2.26 |
| XL-n2541-k121  | 146390  | 146489.1  | -   | 173080.304  | 173080.304  | 18.15 | 2.35     | 165957.035  | 165957.035  | 13.29  | 2.26 |
| XL-n2587-k66   | 73394   | 73520.7   | -   | 98794.314   | 98794.314   | 34.38 | 2.36     | 106069.043  | 106069.043  | 44.27  | 2.34 |
| XL-n2634-k17   | 31641   | 31748.6   | -   | 48032.030   | 48038.150   | 51.31 | 2.37     | 117064.816  | 117066.813  | 268.73 | 2.59 |
| XL-n2681-k540  | 798603  | 798950.4  | -   | 836138.730  | 836515.852  | 4.70  | 2.81     | 864486.694  | 864486.694  | 8.20   | 2.72 |
| XL-n2727-k546  | 431134  | 431173.0  | -   | 447960.149  | 447960.601  | 3.89  | 2.85     | 446338.732  | 446368.405  | 3.52   | 2.77 |
| XL-n2774-k286  | 407847  | 408000.2  | -   | 432051.432  | 432051.432  | 5.89  | 2.71     | 433664.315  | 433679.120  | 6.29   | 2.60 |
| XL-n2821-k208  | 216763  | 216868.8  | -   | 249393.931  | 249897.648  | 15.23 | 2.70     | 249095.933  | 249095.933  | 14.86  | 2.62 |
| XL-n2867-k120  | 165990  | 166056.6  | -   | 185528.860  | 185528.860  | 11.73 | 2.67     | 184467.969  | 184700.004  | 11.23  | 2.58 |
| XL-n2914-k95   | 88990   | 89080.2   | -   | 117204.238  | 117204.238  | 31.57 | 2.69     | 170982.906  | 172218.167  | 93.33  | 2.78 |
| XL-n2961-k55   | 108084  | 108200.9  | -   | 136325.524  | 136325.524  | 25.99 | 2.72     | 137354.465  | 137354.465  | 26.94  | 2.64 |
| XL-n3007-k658  | 522319  | 522458.9  | -   | 567396.203  | 567396.203  | 8.60  | 3.23     | 564897.685  | 565803.048  | 8.30   | 3.14 |
| XL-n3054-k461  | 782739  | 783022.3  | -   | 826035.355  | 826150.600  | 5.51  | 3.11     | 824720.670  | 824843.015  | 5.34   | 3.02 |
| XL-n3101-k311  | 245937  | 246059.9  | -   | 276276.792  | 276276.792  | 12.28 | 3.04     | 287229.828  | 287229.828  | 16.73  | 2.98 |
| XL-n3147-k232  | 256626  | 256746.6  | -   | 281018.618  | 281018.618  | 9.45  | 3.02     | 280283.849  | 280283.849  | 9.17   | 2.94 |
| XL-n3194-k161  | 148728  | 148905.3  | -   | 183576.794  | 183576.794  | 23.28 | 3.01     | 187617.150  | 187617.150  | 26.00  | 2.99 |
| XL-n3241-k115  | 221370  | 221468.2  | -   | 243597.957  | 243597.957  | 9.99  | 3.05     | 243784.846  | 243784.846  | 10.08  | 2.97 |
| XL-n3287-k30   | 40229   | 40264.9   | -   | 58059.840   | 58063.358   | 44.20 | 3.01     | 63246.994   | 63246.994   | 57.08  | 2.98 |
| XL-n3334-k934  | 1452698 | 1452950.7 | -   | 1528764.499 | 1528764.499 | 5.22  | 3.78     | 1551991.614 | 1552231.308 | 6.83   | 3.73 |
| XL-n3408-k524  | 678643  | 678911.7  | -   | 729543.008  | 729543.008  | 7.46  | 3.55     | 730466.570  | 730525.313  | 7.60   | 3.46 |
| XL-n3484-k436  | 703355  | 703416.8  | -   | 725525.712  | 726051.866  | 3.22  | 3.56     | 718160.574  | 718223.322  | 2.10   | 3.47 |
| XL-n3561-k229  | 209386  | 209555.6  | -   | 240160.557  | 240264.080  | 14.65 | 3.46     | 257265.566  | 257437.405  | 22.85  | 3.45 |
| XL-n3640-k211  | 189724  | 189838.6  | -   | 219511.662  | 219597.549  | 15.68 | 3.52     | 224932.923  | 225391.607  | 18.73  | 3.54 |
| XL-n3721-k77   | 162862  | 162970.3  | -   | 194735.655  | 194735.655  | 19.49 | 3.55     | 192459.029  | 192459.029  | 18.09  | 3.46 |
| XL-n3804-k29   | 52885   | 52935.8   | -   | 80860.099   | 80860.099   | 52.75 | 3.56     | 103106.877  | 103106.877  | 94.78  | 3.66 |
| XL-n3888-k1010 | 1880368 | 1882369.0 | -   | 2027323.425 | 2029446.805 | 7.81  | 4.54     | 6830925.140 | 6830925.140 | 262.89 | 6.61 |
| XL-n3975-k687  | 525901  | 526048.1  | -   | 563664.277  | 564386.890  | 7.29  | 4.32     | 594258.522  | 595877.903  | 13.27  | 4.38 |
| XL-n4063-k347  | 548931  | 549115.2  | -   | 587384.967  | 587408.535  | 6.97  | 4.14     | 588112.594  | 588385.047  | 7.15   | 4.11 |
| XL-n4153-k291  | 356034  | 356149.2  | -   | 388500.618  | 388767.082  | 9.16  | 4.19     | 383117.890  | 383117.890  | 7.57   | 4.17 |
| XL-n4245-k203  | 229659  | 229743.2  | -   | 260046.278  | 260046.278  | 13.19 | 4.25     | 257672.415  | 257672.415  | 12.16  | 4.23 |
| XL-n4340-k148  | 244226  | 244431.7  | -   | 274951.359  | 275016.660  | 12.51 | 4.30     | 272878.904  | 272878.904  | 11.64  | 4.26 |
| XL-n4436-k48   | 61477   | 61583.1   | -   | 84074.433   | 84238.603   | 36.79 | 4.33     | 82587.278   | 82705.299   | 34.30  | 4.32 |
| XL-n4535-k1134 | 1203566 | 1203606.7 | -   | 1229575.270 | 1229575.270 | 2.16  | 5.40     | 1213085.938 | 1213204.669 | 0.80   | 5.39 |
| XL-n4635-k790  | 610650  | 610947.8  | -   | 669976.869  | 670479.749  | 9.74  | 5.28     | 709039.743  | 710056.924  | 16.22  | 5.26 |
| XL-n4738-k487  | 760501  | 760787.8  | -   | 805607.886  | 805607.886  | 5.89  | 5.08     | 811552.647  | 811900.572  | 6.72   | 5.08 |
| XL-n4844-k321  | 404652  | 404837.3  | -   | 451626.307  | 451626.307  | 11.56 | 5.08     | 446735.398  | 446838.737  | 10.37  | 5.08 |
| XL-n4951-k203  | 285269  | 285390.1  | -   | 317440.702  | 317440.702  | 11.23 | 5.13     | 316884.348  | 317198.203  | 11.15  | 5.16 |

continued on next page

Table 12. Results on XL instances: 10 independent runs per instance (Part I, continued).

| Instance        | Optimal  |           |     | OD-DEAL-200 |             |       |       | AGFN-200    |             |        |       |
|-----------------|----------|-----------|-----|-------------|-------------|-------|-------|-------------|-------------|--------|-------|
|                 | Best     | Mean      | Gap | Best        | Mean        | Gap   | Time  | Best        | Mean        | Gap    | Time  |
| XL-n5061-k184   | 161629   | 161716.7  | -   | 189609.430  | 189643.793  | 17.27 | 5.22  | 234559.279  | 234559.279  | 45.04  | 5.47  |
| XL-n5174-k55    | 61382    | 61489.1   | -   | 89519.570   | 89519.570   | 45.59 | 5.28  | 179109.877  | 179157.565  | 191.36 | 5.78  |
| XL-n5288-k1246  | 1960101  | 1960957.8 | -   | 2087004.120 | 2087004.120 | 6.43  | 6.60  | 2088156.813 | 2089401.319 | 6.55   | 6.65  |
| XL-n5406-k783   | 1040536  | 1040723.8 | -   | 1085262.252 | 1085262.252 | 4.28  | 6.29  | 1098343.332 | 1098531.867 | 5.55   | 6.37  |
| XL-n5526-k553   | 336898   | 336984.8  | -   | 362834.217  | 363133.871  | 7.76  | 6.25  | 505859.169  | 506517.651  | 50.31  | 7.24  |
| XL-n5649-k401   | 644866   | 644987.8  | -   | 701773.320  | 701916.834  | 8.83  | 6.31  | 695155.927  | 695159.252  | 7.78   | 6.40  |
| XL-n5774-k290   | 250207   | 250337.8  | -   | 300101.860  | 300101.860  | 19.88 | 6.39  | 341155.165  | 341942.581  | 36.59  | 6.68  |
| XL-n5902-k122   | 217447   | 217668.5  | -   | 255770.298  | 255770.509  | 17.50 | 6.39  | 258728.744  | 258728.744  | 18.86  | 6.55  |
| XL-n6034-k61    | 644448   | 64615.0   | -   | 93427.839   | 93897.766   | 45.32 | 6.54  | 327982.880  | 328862.986  | 408.96 | 7.48  |
| XL-n6168-k1922  | 1530010  | 1530476.6 | -   | 1714848.608 | 1715098.927 | 12.06 | 8.60  | 1790399.170 | 1792917.854 | 17.15  | 8.85  |
| XL-n6305-k1042  | 1177528  | 1177837.0 | -   | 1269616.823 | 1270224.360 | 7.84  | 8.01  | 1285960.170 | 1286565.689 | 9.23   | 8.18  |
| XL-n6445-k628   | 996623   | 996804.7  | -   | 1048893.769 | 1048894.741 | 5.23  | 7.74  | 1046790.547 | 1046901.494 | 5.03   | 7.99  |
| XL-n6588-k473   | 334068   | 334232.1  | -   | 378271.408  | 378328.799  | 13.19 | 7.81  | 535443.933  | 536267.731  | 60.45  | 8.81  |
| XL-n6734-k330   | 448031   | 448257.5  | -   | 485879.018  | 485997.352  | 8.42  | 7.93  | 489112.698  | 489369.572  | 9.17   | 8.18  |
| XL-n6884-k148   | 181809   | 181960.4  | -   | 223635.698  | 223742.489  | 22.96 | 7.95  | 215828.738  | 216230.614  | 18.83  | 8.28  |
| XL-n7037-k38    | 70845    | 70906.9   | -   | 107563.035  | 108101.991  | 52.46 | 8.11  | 150046.446  | 150648.252  | 112.46 | 8.75  |
| XL-n7193-k1683  | 2958979  | 2959237.4 | -   | 3123765.346 | 3125691.441 | 5.62  | 10.23 | 3135225.506 | 3136079.699 | 5.98   | 10.68 |
| XL-n7353-k1471  | 1537811  | 1537904.2 | -   | 1578009.158 | 1578009.158 | 2.61  | 10.23 | 1566243.821 | 1566391.713 | 1.85   | 10.68 |
| XL-n7516-k859   | 573902   | 574104.2  | -   | 671712.881  | 674105.531  | 17.42 | 9.89  | 694845.218  | 695419.488  | 21.13  | 10.44 |
| XL-n7683-k602   | 702098   | 702303.9  | -   | 755557.251  | 755593.305  | 7.59  | 9.89  | 753234.365  | 753919.161  | 7.35   | 10.40 |
| XL-n7854-k365   | 659221   | 659311.3  | -   | 752600.720  | 753668.505  | 14.31 | 9.98  | 686270.764  | 686757.389  | 4.16   | 10.52 |
| XL-n8028-k294   | 266900   | 267065.9  | -   | 323032.862  | 323032.862  | 20.96 | 10.16 | 339442.444  | 339635.589  | 27.17  | 10.96 |
| XL-n8207-k108   | 118274   | 118495.5  | -   | 159741.973  | 159742.355  | 34.81 | 7.45  | 151893.973  | 152579.858  | 28.76  | 8.12  |
| XL-n8389-k2028  | 3358731  | 3359593.2 | -   | 3502778.719 | 3504888.816 | 4.32  | 9.21  | 3548488.819 | 3552324.044 | 5.74   | 9.94  |
| XL-n8575-k1297  | 1089137  | 1089360.7 | -   | 1158584.533 | 1158584.533 | 6.35  | 8.79  | 1176872.036 | 1177604.756 | 8.10   | 9.60  |
| XL-n8766-k1032  | 906406   | 906592.3  | -   | 992275.129  | 992883.407  | 9.52  | 8.81  | 978605.185  | 979179.949  | 8.01   | 9.75  |
| XL-n8960-k634   | 773383   | 773515.7  | -   | 829340.036  | 829438.252  | 7.23  | 8.74  | 814260.055  | 814691.224  | 5.32   | 9.60  |
| XL-n9160-k379   | 324092   | 324277.1  | -   | 397820.920  | 397918.517  | 22.71 | 8.78  | 416270.602  | 416936.620  | 28.57  | 9.91  |
| XL-n9363-k209   | 205575   | 205690.5  | -   | 249883.193  | 249883.193  | 21.49 | 8.94  | 437952.626  | 438738.939  | 113.30 | 10.48 |
| XL-n9571-k55    | 106791   | 106987.1  | -   | 155184.828  | 155248.189  | 45.11 | 9.09  | 167567.474  | 167567.474  | 56.62  | 10.14 |
| XL-n9784-k2774  | 4078217  | 4078505.8 | -   | 4270823.202 | 4272518.236 | 4.76  | 11.69 | 4296785.814 | 4300476.672 | 5.44   | 12.75 |
| XL-n10001-k1570 | 2333757  | 2334348.4 | -   | 2536956.911 | 2538263.213 | 8.74  | 11.30 | 2467545.241 | 2469204.674 | 5.78   | 12.22 |
| Average         | 516647.8 | 516827.4  | -   | 561005.408  | 561206.472  | 16.93 | 4.49  | 625852.900  | 626220.662  | 35.95  | 4.67  |

Table 13. Results on XL instances: 10 independent runs per instance (Part II).

| Instance      | Optimal |           |     | GFACS-200  |            |      |      | GLOP       |            |       |      |
|---------------|---------|-----------|-----|------------|------------|------|------|------------|------------|-------|------|
|               | Best    | Mean      | Gap | Best       | Mean       | Gap  | Time | Best       | Mean       | Gap   | Time |
| XL-n1048-k237 | 380211  | 380369.4  | -   | 410047.666 | 410885.386 | 8.02 | 2.73 | 484094.764 | 484094.764 | 27.27 | 1.02 |
| XL-n1094-k157 | 112431  | 112452.6  | -   | 114946.128 | 114946.128 | 2.22 | 2.49 | 164613.895 | 164613.895 | 46.39 | 1.00 |
| XL-n1141-k112 | 95727   | 95798.9   | -   | 101063.659 | 101063.659 | 5.50 | 2.41 | 121436.903 | 121436.903 | 26.76 | 0.99 |
| XL-n1188-k96  | 104415  | 104511.6  | -   | 109002.853 | 109002.853 | 4.30 | 2.43 | 122754.384 | 122754.384 | 17.46 | 1.02 |
| XL-n1234-k55  | 96647   | 96787.3   | -   | 101915.998 | 101915.998 | 5.30 | 2.31 | 121398.054 | 121398.054 | 25.43 | 1.02 |
| XL-n1281-k29  | 31101   | 31174.1   | -   | 33379.131  | 33379.131  | 7.07 | 2.45 | 39248.257  | 39248.257  | 25.90 | 1.02 |
| XL-n1328-k19  | 38247   | 38315.0   | -   | 41324.849  | 41324.849  | 7.86 | 2.44 | 45763.356  | 45763.356  | 19.44 | 1.02 |
| XL-n1374-k278 | 233049  | 233248.0  | -   | 242662.266 | 243616.855 | 4.45 | 3.49 | 357402.880 | 357402.880 | 53.23 | 1.10 |
| XL-n1421-k232 | 384826  | 384949.2  | -   | 398073.594 | 398073.594 | 3.41 | 3.38 | 450774.804 | 450774.804 | 17.10 | 1.09 |
| XL-n1468-k151 | 250166  | 250305.2  | -   | 259065.481 | 259065.481 | 3.50 | 3.12 | 308177.839 | 308177.839 | 23.12 | 1.09 |
| XL-n1514-k106 | 92425   | 92489.7   | -   | 97727.468  | 97727.468  | 5.66 | 3.15 | 117414.436 | 117414.436 | 26.95 | 1.09 |
| XL-n1561-k75  | 101549  | 101583.3  | -   | 104547.191 | 104547.191 | 2.92 | 3.01 | 125094.345 | 125094.345 | 23.14 | 1.10 |
| XL-n1608-k39  | 48021   | 48064.3   | -   | 51358.670  | 51358.670  | 6.85 | 3.23 | 57033.695  | 57033.695  | 18.66 | 1.11 |
| XL-n1654-k111 | 36385   | 36429.1   | -   | 40015.119  | 40015.119  | 9.84 | 2.97 | 43967.344  | 43967.344  | 20.69 | 1.11 |
| XL-n1701-k562 | 521136  | 521380.5  | -   | 548682.329 | 548682.329 | 5.24 | 5.34 | 656249.245 | 656249.245 | 25.87 | 1.27 |
| XL-n1748-k271 | 173896  | 174027.2  | -   | 181737.618 | 182085.308 | 4.63 | 4.22 | 221879.574 | 221879.574 | 27.50 | 1.18 |
| XL-n1794-k163 | 141729  | 141777.6  | -   | 147081.507 | 147081.507 | 3.74 | 3.80 | 195759.271 | 195759.271 | 38.07 | 1.17 |
| XL-n1841-k126 | 214038  | 214142.6  | -   | 223761.983 | 224218.976 | 4.71 | 3.88 | 261325.385 | 261325.385 | 22.03 | 1.19 |
| XL-n1888-k82  | 143623  | 143733.5  | -   | 150829.253 | 150829.253 | 4.94 | 3.65 | 175909.082 | 175909.082 | 22.39 | 1.18 |
| XL-n1934-k46  | 53013   | 53067.3   | -   | 56259.990  | 56259.990  | 6.02 | 3.78 | 64714.653  | 64714.653  | 21.95 | 1.19 |
| XL-n1981-k13  | 32580   | 32639.1   | -   | 35252.869  | 35252.869  | 8.01 | 3.76 | 40725.828  | 40725.828  | 24.78 | 1.19 |
| XL-n2028-k617 | 544403  | 5444596.6 | -   | 569391.400 | 569391.400 | 4.55 | 6.16 | 691281.903 | 691281.903 | 26.93 | 1.36 |
| XL-n2074-k264 | 421627  | 421805.0  | -   | 435731.755 | 435731.755 | 3.30 | 4.88 | 563030.258 | 563030.258 | 33.48 | 1.26 |
| XL-n2121-k186 | 283211  | 283323.6  | -   | 291878.712 | 291878.712 | 3.02 | 4.67 | 357266.422 | 357266.422 | 26.10 | 1.25 |
| XL-n2168-k138 | 127298  | 127450.2  | -   | 134457.086 | 134457.086 | 5.50 | 4.83 | 172137.170 | 172137.170 | 35.06 | 1.29 |
| XL-n2214-k131 | 154676  | 154722.4  | -   | 158962.654 | 159002.749 | 2.77 | 4.60 | 191546.631 | 191546.631 | 23.80 | 1.27 |

continued on next page

Table 13. Results on XL instances: 10 independent runs per instance (Part II, continued).

| Instance       | Optimal |           |     | GFACS-200   |             |       | GLOP  |             |             |       |      |
|----------------|---------|-----------|-----|-------------|-------------|-------|-------|-------------|-------------|-------|------|
|                | Best    | Mean      | Gap | Best        | Mean        | Gap   | Time  | Best        | Mean        | Gap   | Time |
| XL-n2261-k54   | 98907   | 98993.6   | -   | 105903.509  | 105912.237  | 6.99  | 4.42  | 118271.139  | 118271.139  | 19.47 | 1.28 |
| XL-n2307-k34   | 47958   | 48020.2   | -   | 52271.676   | 52271.676   | 8.85  | 4.81  | 57782.033   | 57782.033   | 20.33 | 1.29 |
| XL-n2354-k631  | 940825  | 940960.9  | -   | 975806.598  | 977760.490  | 3.91  | 7.21  | 1114872.523 | 1114872.523 | 18.48 | 1.47 |
| XL-n2401-k408  | 463473  | 463673.4  | -   | 481430.520  | 481901.606  | 3.93  | 6.09  | 694990.321  | 694990.321  | 49.89 | 1.39 |
| XL-n2447-k290  | 218706  | 218821.4  | -   | 234992.841  | 236226.151  | 7.95  | 5.92  | 330987.113  | 330987.113  | 51.26 | 1.42 |
| XL-n2494-k194  | 361205  | 361273.1  | -   | 370246.280  | 370246.280  | 2.48  | 5.50  | 400620.322  | 400620.322  | 10.89 | 1.39 |
| XL-n2541-k121  | 146390  | 146489.1  | -   | 152992.436  | 153063.893  | 4.49  | 5.61  | 183797.906  | 183797.906  | 25.47 | 1.37 |
| XL-n2587-k66   | 73394   | 73520.7   | -   | 78977.126   | 79032.246   | 7.50  | 5.76  | 83094.056   | 83094.056   | 13.02 | 1.36 |
| XL-n2634-k17   | 31641   | 31748.6   | -   | 34994.477   | 35177.319   | 10.80 | 5.95  | 41241.794   | 41241.794   | 29.90 | 1.37 |
| XL-n2681-k540  | 798603  | 798950.4  | -   | 830208.541  | 831553.020  | 4.08  | 7.38  | 998524.506  | 998524.506  | 24.98 | 1.50 |
| XL-n2727-k546  | 431134  | 431173.0  | -   | 439113.228  | 439216.754  | 1.87  | 7.79  | 666447.417  | 666447.417  | 54.57 | 1.56 |
| XL-n2774-k286  | 407847  | 408000.2  | -   | 419917.107  | 419921.721  | 2.92  | 6.65  | 503074.608  | 503074.608  | 23.30 | 1.46 |
| XL-n2821-k208  | 216763  | 216868.8  | -   | 229484.215  | 230179.149  | 6.14  | 6.72  | 303208.394  | 303208.394  | 39.81 | 1.49 |
| XL-n2867-k120  | 165990  | 166056.6  | -   | 173014.131  | 173035.903  | 4.20  | 6.42  | 206107.314  | 206121.484  | 24.13 | 1.46 |
| XL-n2914-k95   | 88990   | 89080.2   | -   | 95154.432   | 95154.432   | 6.82  | 6.54  | 113836.997  | 113836.997  | 27.79 | 1.50 |
| XL-n2961-k55   | 108084  | 108200.9  | -   | 117962.585  | 117962.585  | 9.02  | 6.19  | 129369.744  | 129369.744  | 19.56 | 1.48 |
| XL-n3007-k658  | 522319  | 522458.9  | -   | 542638.163  | 543853.031  | 4.09  | 8.59  | 759304.871  | 759304.871  | 45.33 | 1.73 |
| XL-n3054-k461  | 782739  | 783022.3  | -   | 808441.660  | 808441.660  | 3.25  | 7.90  | 929001.042  | 929001.042  | 18.64 | 1.71 |
| XL-n3101-k311  | 245937  | 246059.9  | -   | 262390.651  | 263178.679  | 6.96  | 7.42  | 339472.082  | 339472.082  | 37.96 | 1.70 |
| XL-n3147-k232  | 256626  | 256746.6  | -   | 266387.193  | 266731.508  | 3.89  | 7.38  | 348454.409  | 348454.409  | 35.72 | 1.63 |
| XL-n3194-k161  | 148728  | 148905.3  | -   | 157767.627  | 157797.546  | 5.97  | 7.48  | 199446.978  | 199446.978  | 33.94 | 1.69 |
| XL-n3241-k115  | 221370  | 221468.2  | -   | 230501.837  | 230501.837  | 4.08  | 7.08  | 254192.368  | 254192.368  | 14.78 | 1.67 |
| XL-n3287-k30   | 40229   | 40264.9   | -   | 44526.420   | 44526.420   | 10.58 | 6.97  | 48236.421   | 48236.421   | 19.80 | 1.64 |
| XL-n3334-k934  | 1452698 | 1452950.7 | -   | 1496610.057 | 1499123.522 | 3.18  | 10.95 | 1769752.471 | 1769752.471 | 21.80 | 1.97 |
| XL-n3408-k524  | 678643  | 678911.7  | -   | 703547.512  | 704701.345  | 3.80  | 9.61  | 936860.003  | 938116.879  | 38.18 | 1.79 |
| XL-n3484-k436  | 703355  | 703416.8  | -   | 708964.632  | 709250.383  | 0.83  | 8.74  | 815048.530  | 815048.530  | 15.87 | 1.79 |
| XL-n3561-k229  | 209386  | 209555.6  | -   | 219119.496  | 219119.496  | 4.56  | 8.56  | 289927.766  | 289927.766  | 38.35 | 1.79 |
| XL-n3640-k211  | 189724  | 189838.6  | -   | 199776.614  | 199776.614  | 5.23  | 8.74  | 255503.720  | 255503.720  | 34.59 | 1.81 |
| XL-n3721-k77   | 162862  | 162970.3  | -   | 171803.517  | 171803.517  | 5.42  | 8.28  | 192025.850  | 192025.850  | 17.83 | 1.79 |
| XL-n3804-k29   | 52885   | 52935.8   | -   | 59028.641   | 59030.626   | 11.51 | 8.57  | 63431.817   | 63431.817   | 19.83 | 1.81 |
| XL-n3888-k1010 | 1880368 | 1882369.0 | -   | 2056632.110 | 2056632.110 | 9.26  | 13.57 | 2283262.054 | 2283262.054 | 21.30 | 2.36 |
| XL-n3975-k687  | 525901  | 526048.1  | -   | 545187.877  | 545448.010  | 3.69  | 11.46 | 768913.176  | 768913.176  | 46.17 | 2.02 |
| XL-n4063-k347  | 548931  | 549115.2  | -   | 567435.378  | 567435.378  | 3.34  | 10.11 | 770746.846  | 770746.846  | 40.36 | 1.98 |
| XL-n4153-k291  | 356034  | 356149.2  | -   | 365915.767  | 366024.789  | 2.77  | 10.23 | 442909.426  | 442909.426  | 24.36 | 1.98 |
| XL-n4245-k203  | 229659  | 229743.2  | -   | 239303.776  | 239303.776  | 4.16  | 10.50 | 289038.521  | 289038.521  | 25.81 | 1.99 |
| XL-n4340-k148  | 244226  | 244431.7  | -   | 258527.810  | 259130.741  | 6.01  | 9.97  | 313912.465  | 313912.465  | 28.43 | 2.01 |
| XL-n4436-k48   | 61477   | 61583.1   | -   | 67049.758   | 67078.934   | 8.92  | 10.15 | 71369.545   | 71369.545   | 15.89 | 2.01 |
| XL-n4535-k1134 | 1203566 | 1203606.7 | -   | 1209342.241 | 1209640.752 | 0.50  | 15.11 | 1341343.969 | 1341343.969 | 11.44 | 2.41 |
| XL-n4635-k790  | 610650  | 610947.8  | -   | 635809.014  | 636298.648  | 4.15  | 13.80 | 912708.890  | 912708.890  | 49.39 | 2.34 |
| XL-n4738-k487  | 760501  | 760787.8  | -   | 786627.508  | 786627.508  | 3.40  | 13.16 | 1057036.482 | 1057036.482 | 38.94 | 2.29 |
| XL-n4844-k321  | 404652  | 404837.3  | -   | 423490.345  | 424342.250  | 4.82  | 12.83 | 485131.089  | 485131.089  | 19.83 | 2.35 |
| XL-n4951-k203  | 285269  | 285390.1  | -   | 298293.911  | 298888.098  | 4.73  | 12.46 | 389854.618  | 389854.618  | 36.60 | 2.24 |
| XL-n5061-k184  | 161629  | 161716.7  | -   | 169022.548  | 169022.548  | 4.52  | 13.52 | 202703.771  | 202703.771  | 25.34 | 2.38 |
| XL-n5174-k55   | 61382   | 61489.1   | -   | 68913.417   | 68913.417   | 12.07 | 13.39 | 76827.832   | 76827.832   | 24.95 | 2.36 |
| XL-n5288-k1246 | 1960101 | 1960957.8 | -   | 2034919.833 | 2036505.090 | 3.85  | 19.05 | 2290037.069 | 2290037.069 | 16.78 | 2.85 |
| XL-n5406-k783  | 1040536 | 1040723.8 | -   | 1066362.031 | 1067220.870 | 2.55  | 17.21 | 1181510.583 | 1181510.583 | 13.53 | 2.67 |
| XL-n5526-k553  | 336898  | 336984.8  | -   | 345878.761  | 346070.057  | 2.70  | 16.52 | 488843.255  | 488843.255  | 45.06 | 2.61 |
| XL-n5649-k401  | 644866  | 644987.8  | -   | 674554.631  | 675488.157  | 4.73  | 16.07 | 869332.948  | 869332.948  | 34.78 | 2.65 |
| XL-n5774-k290  | 250207  | 250337.8  | -   | 263124.427  | 263124.427  | 5.11  | 16.21 | 356104.326  | 356104.326  | 42.25 | 2.66 |
| XL-n5902-k122  | 217447  | 217668.5  | -   | 234572.804  | 234572.804  | 7.77  | 15.72 | 273776.058  | 273776.058  | 25.78 | 2.69 |
| XL-n6034-k61   | 64448   | 64615.0   | -   | 72005.619   | 72114.132   | 11.61 | 16.70 | 82108.585   | 82108.585   | 27.07 | 2.68 |
| XL-n6168-k1922 | 1530010 | 1530476.6 | -   | 1606833.820 | 1606833.820 | 4.99  | 24.76 | 2105143.644 | 2105143.644 | 37.55 | 3.49 |
| XL-n6305-k1042 | 1177528 | 1177837.0 | -   | 1229612.265 | 1231137.969 | 4.53  | 21.78 | 1645893.829 | 1645893.829 | 39.74 | 3.13 |
| XL-n6445-k628  | 996623  | 996804.7  | -   | 1023096.201 | 1023096.201 | 2.64  | 20.15 | 1217675.532 | 1217675.532 | 22.16 | 3.02 |
| XL-n6588-k473  | 334068  | 334232.1  | -   | 346063.135  | 346063.135  | 3.54  | 19.98 | 490939.358  | 490939.358  | 46.89 | 3.05 |
| XL-n6734-k330  | 448031  | 448257.5  | -   | 464107.187  | 464107.187  | 3.54  | 20.95 | 562865.090  | 562865.090  | 25.57 | 3.10 |
| XL-n6884-k148  | 181809  | 181960.4  | -   | 192823.342  | 192823.342  | 5.97  | 20.15 | 237574.881  | 237574.881  | 30.56 | 3.07 |
| XL-n7037-k38   | 70845   | 70906.9   | -   | 80534.192   | 80534.192   | 13.58 | 20.90 | 85876.862   | 85876.862   | 21.11 | 3.09 |
| XL-n7193-k1683 | 2958979 | 2959237.4 | -   | 3048064.812 | 3049608.204 | 3.05  | 29.05 | 3357072.604 | 3357072.604 | 13.44 | 3.77 |
| XL-n7353-k1471 | 1537811 | 1537904.2 | -   | 1562714.121 | 1563810.948 | 1.68  | 27.74 | 2180165.318 | 2180165.318 | 41.76 | 3.87 |
| XL-n7516-k859  | 573902  | 574104.2  | -   | 593204.034  | 593525.592  | 3.38  | 25.87 | 755025.555  | 755025.555  | 31.51 | 3.58 |
| XL-n7683-k602  | 702098  | 702303.9  | -   | 722963.045  | 722963.045  | 2.94  | 25.80 | 839488.251  | 839488.251  | 19.53 | 3.51 |
| XL-n7854-k365  | 659221  | 659311.3  | -   | 674679.005  | 675037.095  | 2.39  | 25.88 | 740458.586  | 740458.586  | 12.37 | 3.64 |
| XL-n8028-k294  | 266900  | 267065.9  | -   | 283818.210  | 284298.472  | 6.45  | 26.73 | 484388.795  | 484388.795  | 81.37 | 3.68 |
| XL-n8207-k108  | 118274  | 118495.5  | -   | 126883.776  | 126883.776  | 7.08  | 25.89 | 141843.523  | 141843.523  | 19.70 | 3.64 |
| XL-n8389-k2028 | 3358731 | 3359593.2 | -   | 3503368.892 | 3509642.209 | 4.47  | 35.82 | 3991783.671 | 3991783.671 | 18.82 | 4.46 |
| XL-n8575-k1297 | 1089137 | 1089360.7 | -   | 1121060.492 | 1121060.492 | 2.91  | 32.11 | 1453584.882 | 1453584.882 | 33.43 | 4.21 |
| XL-n8766-k1032 | 906406  | 906592.3  | -   | 936845.928  | 936845.928  | 3.34  | 32.44 | 1238717.215 | 1238717.215 | 36.64 | 4.14 |

continued on next page

*Table 13.* Results on XL instances: 10 independent runs per instance (Part II, continued).

| Instance        | Optimal  |           |     | GFACS-200   |             |       | GLOP  |             |             |       |      |
|-----------------|----------|-----------|-----|-------------|-------------|-------|-------|-------------|-------------|-------|------|
|                 | Best     | Mean      | Gap | Best        | Mean        | Gap   | Time  | Best        | Mean        | Gap   | Time |
| XL-n8960-k634   | 773383   | 773515.7  | -   | 792238.944  | 792492.228  | 2.45  | 32.14 | 1013665.958 | 1013665.958 | 31.05 | 4.16 |
| XL-n9160-k379   | 324092   | 324277.1  | -   | 344480.087  | 344779.984  | 6.32  | 33.10 | 567033.168  | 567033.168  | 74.86 | 4.29 |
| XL-n9363-k209   | 205575   | 205690.5  | -   | 218353.910  | 218389.472  | 6.17  | 32.63 | 253397.867  | 253397.867  | 23.19 | 4.23 |
| XL-n9571-k55    | 106791   | 106987.1  | -   | 123088.378  | 123088.378  | 15.05 | 33.65 | 132965.804  | 132965.804  | 24.28 | 4.41 |
| XL-n9784-k2774  | 4078217  | 4078505.8 | -   | 4192740.055 | 4195398.099 | 2.87  | 48.62 | 4872880.461 | 4872910.355 | 19.48 | 5.50 |
| XL-n10001-k1570 | 2333757  | 2334348.4 | -   | 2408873.017 | 2408873.017 | 3.19  | 43.30 | 2814800.153 | 2815859.101 | 20.63 | 4.67 |
| Average         | 516647.8 | 516827.4  | -   | 536825.474  | 537194.212  | 5.22  | 12.56 | 654285.974  | 654314.320  | 28.85 | 2.14 |

#### D.4. Supplemental TSP Benchmarks

*Table 14.* Overall performance comparison on the synthetic TSP dataset. The *Obj.* indicates the average total travel distance, while *Time* denotes the average time required to solve a single instance. The best results are highlighted in bold and the second-best results are indicated with underlining.

| Method       | V  = 200         |             |             | V  = 500         |              |             | V  = 1000        |             |             |
|--------------|------------------|-------------|-------------|------------------|--------------|-------------|------------------|-------------|-------------|
|              | Obj.             | Gap (%)     | Time (s)    | Obj.             | Gap (%)      | Time (s)    | Obj.             | Gap (%)     | Time (s)    |
| LKH-3(100)   | 10.724371        | —           | 0.40        | 16.606491        | —            | 1.04        | 23.282794        | —           | 2.05        |
| LKH-3(1000)  | 10.719438        | -0.05       | 2.11        | 16.562766        | -0.26        | 5.12        | 23.177903        | -0.45       | 11.17       |
| LKH-3(10000) | 10.719180        | -0.05       | 10.87       | 16.551830        | -0.33        | 26.16       | 23.143115        | -0.60       | 54.74       |
| POMO         | 10.887800        | 1.52        | <b>0.05</b> | 20.181600        | 21.53        | 0.47        | 32.505500        | 39.61       | 3.66        |
| NeuOpt       | <b>10.837507</b> | <b>1.05</b> | 0.45        | 55.235378        | 232.61       | 1.34        | 277.531128       | 1092.00     | 3.61        |
| GLOP         | <u>10.856474</u> | 1.23        | 0.09        | <b>16.908892</b> | <b>1.82</b>  | 0.62        | <b>23.837715</b> | <b>2.38</b> | <u>1.25</u> |
| OD-DEAL-200  | 11.665637        | 8.78        | <u>0.06</u> | 18.476112        | <u>11.26</u> | <b>0.16</b> | 28.419750        | 22.06       | <b>0.40</b> |
| ACO          | <u>11.505671</u> | <u>7.29</u> | 3.39        | 17.970035        | <u>8.21</u>  | 34.89       | <u>25.137234</u> | <u>7.96</u> | 266.98      |
| GFACS        | <b>10.801056</b> | <b>0.72</b> | 0.15        | <b>16.957058</b> | <b>2.11</b>  | 0.78        | <b>23.949020</b> | <b>2.86</b> | 4.32        |
| AGFN-200     | 11.841615        | 10.42       | <u>0.09</u> | 18.568083        | 11.81        | <u>0.21</u> | 26.460453        | 13.65       | <u>0.41</u> |
| AGFN-500     | 12.041571        | 12.28       | <u>0.09</u> | 18.790956        | 13.15        | <u>0.21</u> | 26.460077        | 13.65       | <u>0.41</u> |
| AGFN-1000    | 12.274513        | 14.45       | 0.12        | 19.237740        | 15.84        | 0.28        | 27.059122        | 16.22       | 0.50        |
| OD-DEAL-200  | 11.665637        | 8.78        | <b>0.06</b> | 18.476112        | 11.26        | <b>0.16</b> | 28.419750        | 22.06       | <b>0.40</b> |
| OD-DEAL-500  | 11.728203        | 9.36        | <b>0.06</b> | 18.708435        | 12.66        | <b>0.16</b> | 29.465239        | 26.55       | <b>0.40</b> |
| OD-DEAL-1000 | 12.740256        | 18.80       | <b>0.06</b> | 19.815060        | 19.32        | <b>0.16</b> | 30.033415        | 28.99       | <b>0.40</b> |

This subsection presents a comparative evaluation of OD-DEAL against SOTA baselines for the traveling salesman problem (TSP).

**Baselines:** Following the evaluation protocol established for the CVRP, we benchmark OD-DEAL against a diverse set of traditional and neural solvers for the TSP. Consistent with the CVRP setting, we utilize LKH-3 (Helsgaun, 2000), POMO (Kwon et al., 2020), and NeuOpt (Ma et al., 2024) as fixed small-scale training baselines (**upper half** of Table 14). We further include ACO (Mazzeo & Loiseau, 2004) and GFACS (Kim et al., 2025) to evaluate performance under varying training scales (**lower half** of Table 14). Furthermore, we report results for AGFN and OD-DEAL variants trained on instances with 200, 500, and 1000 nodes. All test datasets consist of synthetic TSP instances with 200, 500, and 1000 nodes, where node coordinates are uniformly sampled from the unit square  $[0, 1]^2$ .

**Result:** The experimental results, summarized in Table 14, reveal distinct performance trends regarding model generalization, computational efficiency, and architectural specificity.

*Generalization of Fixed-Scale Solvers.* As illustrated in the **upper half** of Table 14, existing fixed-scale neural baselines exhibit limited generalization and a sharp degradation in inference efficiency on large-scale TSP instances. While POMO achieves competitive performance at 200 nodes (1.52% optimal gap), but its gap increases to 39.61% at 1,000 nodes, with inference time rising to 3.66 seconds. NeuOpt suffers from catastrophic failure on massive geometric topologies, yielding a gap exceeding 1000% at 1,000 nodes. In contrast, OD-DEAL-200 demonstrates superior generalization and efficiency. At 1,000 nodes, it achieves an optimality gap of 22.06%, significantly outperforming POMO while requiring only 0.40 seconds for inference, representing a nearly nine-fold speedup.

*Efficiency and Scalability Trade-offs.* The comparative analysis against multi-scale solvers in the **lower half** of Table 14 further highlights the efficiency of OD-DEAL. While GFACS achieves the lowest optimality gap (2.86% at 1000

nodes), it incurs significant computational overhead, with latency reaching 4.32 seconds. Similarly, although ACO yields high-quality solutions, its prohibitive runtime (266.98s) precludes its use in real-time applications. In contrast, OD-DEAL variants consistently maintain inference times below 0.40 seconds, delivering over a  $10 \times$  speedup compared to GFACS. Although the solution quality of OD-DEAL (gaps of 22.06%–28.99%) is slightly lower than that of heuristics specialized for pure geometric constraints, the framework successfully circumvents the computational bottlenecks that typically plague large-scale solvers.

*Architectural Discussion: From TSP to CVRP.* While OD-DEAL maintains sub-second inference speeds across all TSP scales, its optimality gap increases relative to its performance on CVRP. This discrepancy provides empirical validation of the structural inductive bias inherent in our architecture. The GAT-based generator is specifically engineered to model the heterogeneous interdependencies of the CVRP, particularly the complex coupling spatial proximity, heterogeneous customer demands, and residual vehicle capacity. In contrast, the TSP represents a degenerate case governed solely by geometric distances, resulting in a homogeneous graph structure. In such weakly constrained environments, the attention mechanism lacks the high-dimensional “feature anchors” necessary to precisely lock onto critical topological patterns. These results underscore that OD-DEAL is not a generic pathfinder, but a specialized solver optimized for large-scale logistics routing characterized by high-dimensional feature interactions and complex constraint satisfaction.

## E. Standardized Notations and Baselines

### E.1. Summary of Mathematical Notations

To clearly present the mathematical formulation of the problem and the proposed OD-DEAL framework, Table 15 summarizes the primary notations used in this paper and their definitions.

Table 15. Summary of major mathematical notations.

| Symbol                    | Definition and Description                                                              |
|---------------------------|-----------------------------------------------------------------------------------------|
| <i>Problem Definition</i> |                                                                                         |
| $G(V, E)$                 | Complete graph for CVRP or TSP, where $V$ is the node set and $E$ is the edge set       |
| $V_c$                     | Set of customer nodes $\{v_1, \dots, v_N\}$                                             |
| $v_0$                     | Depot node                                                                              |
| $N$                       | Total number of customer nodes                                                          |
| $c_{ij}$                  | Euclidean distance or travel cost associated with edge $(i, j)$                         |
| $d_i$                     | Demand of node $i$                                                                      |
| $K$                       | Total number of available vehicles                                                      |
| $Q$                       | Maximum capacity of a vehicle                                                           |
| $x_{ij}$                  | Binary decision variable; 1 if a vehicle travels directly from $i$ to $j$ , 0 otherwise |
| $u_i$                     | Auxiliary variable representing accumulated load or visitation order at node $i$        |
| <i>OD-DEAL Model</i>      |                                                                                         |
| $\pi_\theta$              | Generator policy network parameterized by $\theta$                                      |
| $D_\phi$                  | Discriminator network parameterized by $\phi$                                           |
| $P_E$                     | Expert policy distribution (constructed via HGS and BCC decomposition)                  |
| $S_{\text{student}}$      | Student solution generated by the generator                                             |
| $S_{\text{expert}}$       | Expert solution generated by the expert system                                          |
| $h_i$                     | High-dimensional embedding vector of node $i$ (generated by GAT encoder)                |
| $\alpha_{ij}$             | Attention coefficient representing the importance weight of node $j$ to node $i$        |
| $R(S)$                    | Surrogate reward signal for solution $S$ defined by the discriminator output            |
| $\mathcal{L}_{TB}$        | Trajectory Balance Loss                                                                 |
| $\mathcal{L}_D$           | Discriminator Loss Function                                                             |

### E.2. Baseline Algorithm Descriptions

To validate the performance of OD-DEAL, we selected seven representative algorithms as baselines, covering traditional heuristics, constructive neural solvers, and GFlowNet-based generative methods. This section describes the core features, applicability, and source code repositories used in our experiments. Remaining baselines utilize the default parameter configurations established in their respective publications.

**LKH-3.** LKH-3 (Helsgaun, 2000) is a classical heuristic algorithm based on an improved version of the Lin-Kernighan-Helsgaun heuristic. It is widely regarded as a strong baseline in the VRP field capable of generating near-optimal solutions. However, as a purely heuristic method lacking neural dependencies, its computational time grows exponentially with problem size, making it impractical for instances with 10000 nodes within reasonable time limits.

*Source Code:* <https://github.com/c4v4/LKH3>.

**ACO.** ACO (Mazzeo & Loiseau, 2004) is a metaheuristic inspired by the collective foraging behavior of ant colonies, designed to identify high-quality solutions through iterative pheromone updates and probabilistic path construction. While robust across various combinatorial tasks, ACO is characterized by high computational complexity and slow convergence rates. On large-scale instances, the algorithm frequently exhibits premature convergence to local optima and requires extensive parameter tuning, making it significantly less efficient than end-to-end neural architectures for real-time deployment.

*Source Code:* <https://github.com/Smmehdihosseini/AntCVRP>.

**POMO.** POMO (Kwon et al., 2020) is a representative neural constructive solver based on the Transformer architecture. It utilizes the REINFORCE algorithm and enhances solution quality through policy augmentation via multiple optimal rollouts. While POMO achieves fast inference, its generalization ability degrades significantly on large-scale instances (beyond 100 nodes), and it is computationally limited by the quadratic complexity of its self-attention mechanism.

*Source Code:* <https://github.com/yd-kwon/POMO>.

**NeuOpt.** NeuOpt (Ma et al., 2024) is a neural improvement heuristic that enhances constructive solvers through a flexible  $k$ -opt neural search mechanism designed to refine local route structures. While NeuOpt achieves competitive accuracy on small-scale benchmarks, it incurs substantial computational overhead and faces significant scalability challenges, often becoming impractical for instances exceeding 1,000 nodes.

*Source Code:* <https://github.com/yining043/NeuOpt>.

**GFACS.** GFACS (Kim et al., 2025) is a hybrid solver that combines GFlowNet with ant colony optimization (ACO), leveraging the generative capability of GFlowNet to guide the search process. While this synergy enhances solution diversity, the framework's heavy reliance on ACO for iterative refinement introduces significant computational overhead. Consequently, GFACS suffers from high inference latency and exhibits limited scalability on large-scale instances, where the stochastic search phase becomes a bottleneck compared to end-to-end neural solvers.

*Source Code:* <https://github.com/hyeok9855/gfacs>.

**AGFN.** AGFN (Zhang et al., 2025) integrates adversarial training with flow matching to provide denser training signals and enhance solution diversity compared to traditional RL approaches. However, AGFN improves solution diversity, it lacks the structural inductive biases and expert regularization required for large-scale optimization. By neglecting local signals in favor of holistic objectives, such solvers fail to capture fine-grained structures, resulting in suboptimal performance ceilings and reduced training stability.

*Source Code:* <https://github.com/ZHANG-NI/AGFN>.

**GLOP.** GLOP (Ye et al., 2024) is a hierarchical framework that addresses massive routing by integrating global partitioning with local construction. The architecture decomposes instances into a hierarchy of subproblems. Specifically, the model combines nonautoregressive partitioning with autoregressive solvers to address TSPs and shortest Hamiltonian path problems, balancing scalability and route quality. While GLOP delivers strong real-time performance on massive graphs, its multi-stage pipeline necessitates higher modeling complexity relative to end-to-end neural solvers.

*Source Code:* <https://github.com/henry-yeh/GLOP>.

## F. Further Discussion and Limitations

The following discussion evaluates the scalability of OD-DEAL, highlights its limitations, and outlines directions for future research.

**Performance and Scalability.** The OD-DEAL framework successfully overcomes generalization bottlenecks for neural solvers in large-scale CVRP. By integrating dynamic expert guidance with online decomposition, the model achieves a superior balance of solution quality and inference efficiency across complex topologies at ten thousand node scales. The

results demonstrate that neural policies can internalize sophisticated partitioning logic to handle massive combinatorial complexity without explicit clustering at runtime.

**Methodological Limitations.** OD-DEAL demonstrates robust performance in highly constrained optimization. Specific boundary conditions persist for distinct problem classes. Tasks dominated by pure geometric constraints, such as the TSP, reveal performance gaps compared to specialized geometric partitioning algorithms. Current inductive biases for simple, non-capacitated topologies warrant further streamlining. The current generative architecture internalizes decomposition logic implicitly. Integrating explicit clustering rewards provides a mechanism to enhance latent space partitioning efficiency.

**Generalization to Complex Constraints.** Future work will expand the applicability of OD-DEAL to scenarios involving more intricate real-world constraints (Jiao et al., 2024). This includes the CVRP with Time Windows and the pickup and delivery problem. Evaluation on these variants will enable broader verification of architectural generalization and robustness across diverse logistics requirements.

**Practical Utility and Impact.** OD-DEAL demonstrates significant potential for immediate deployment in the service sector. Sub-second inference capabilities support dynamic scenarios requiring real-time responses. Primary application domains include instant delivery, ride-hailing optimization, and service scheduling. The framework establishes a scalable paradigm for large-scale, real-time optimization. This methodology enhances operational management across diverse service industries. The research advances the practical frontiers of neural combinatorial optimization in real-world service applications.